Titre: Title:	Towards Near-Infrared Photosensitization of Tungsten Trioxide Nanostructured Films by Upconverting Nanoparticles
Auteur: Author:	Frédéric Venne
Date:	2015
Type:	Mémoire ou thèse / Dissertation or Thesis
Référence: Citation:	Venne, F. (2015). Towards Near-Infrared Photosensitization of Tungsten Trioxide Nanostructured Films by Upconverting Nanoparticles [Mémoire de maîtrise, École Polytechnique de Montréal]. PolyPublie. https://publications.polymtl.ca/1870/

URL de PolyPublie: PolyPublie URL:	https://publications.polymtl.ca/1870/
Directeurs de recherche: Advisors:	Clara Santato
Programme: Program:	Génie physique

UNIVERSITÉ DE MONTRÉAL

TOWARDS NEAR-INFRARED PHOTOSENSITIZATION OF TUNGSTEN TRIOXIDE NANOSTRUCTURED FILMS BY UPCONVERTING NANOPARTICLES

FRÉDÉRIC VENNE
DÉPARTEMENT DE GÉNIE PHYSIQUE
ÉCOLE POLYTECHNIQUE DE MONTRÉAL

MÉMOIRE PRÉSENTÉ EN VUE DE L'OBTENTION
DU DIPLÔME DE MAÎTRISE ÈS SCIENCES APPLIQUÉES
(GÉNIE PHYSIQUE)
JUILLET 2015

UNIVERSITÉ DE MONTRÉAL

ÉCOLE POLYTECHNIQUE DE MONTRÉAL

Ce mémoire intitulé:

TOWARDS NEAR-INFRARED PHOTOSENSITIZATION OF TUNGSTEN TRIOXIDE NANOSTRUCTURED FILMS BY UPCONVERTING NANOPARTICLES

présenté par: VENNE Frédéric
en vue de l'obtention du diplôme de: Maîtrise ès sciences appliquées
a été dûment accepté par le jury d'examen constitué de:

M. PETER Yves-Alain, Doctorat, président
Mme SANTATO Clara, Doctorat, membre et directrice de recherche
M. MOUTANABBIR Oussama, Ph. D., membre

DEDICATION

À Audrey

ACKNOWLEDGMENTS

Foremost, I would like to thank Prof. Clara Santato for accepting me into her research group, and providing me a highly stimulating opportunity. Thanks for your remarkable availability, scientific rigor, and constant support. I would also like to thank the members of the jury, Prof. Oussama Moutanabbir and Prof. Yves-Alain Peter, who kindly accepted to review this master's thesis.

I would like to thank my close collaborators on this project, Prof. Fiorenzo Vetrone, and Dr. Marta Quintanilla, for their expertise and scientific contribution. I acknowledge the work done by Dr. Dilek Isik, a former graduate student in the group who started the investigation on upconverting nanoparticles a few years ago. I would also like to thank Dr. Bill Baloukas and Hubert Camirand for the discussions we had on tungsten trioxide, and Yves Drolet, Francis Boutet, Jean-Paul Lévesque, Joël Bouchard, and Christophe Clément for the technical support. You are magicians: research would not work without you. Thanks also to Patricia Moraille for the help with the atomic force microscope, and Jeremy Lerner (president at LightForm, Inc) for fruitful discussions about the hyperspectral imaging system.

A thought goes to the Santato's team and all the people working in room PJAB-3076. Thanks Eduardo, Jonathan, Francis, Xuri, Tian, Shiming, and Xiang for the convivial atmosphere, and support (scientific or moral!). I would like to show my gratitude to the visiting students for the stimulating discussions: Kestutis, Martin, and Gustavo. Some people that are now gone, but still marked my master's experience: Julia, Sareh, and Umar. Thanks also to the people working in Prof. Fabio Cicoira's research group (Prajwal, Olga, Irina, Zhihui) for providing me valuable comments on presentations made during joint group meetings. Thanks also to the several summer students in the group. Please acccept my apologies for not remembering all your names.

I would like to thank the coffee addicts Jean-Hughes, Joseph, and Martin for the stimulating and interesting discussions we had around the coffee machine. Thanks to Christian Majeau for his cheerfulness: it is always a pleasure to meet you at the lobby at the beginning of a day. I would like to thank my family for teaching me that hard work and education are the motor of change. I owe a lot to N. Cartier: I never said thank you for the toolbox. My thoughts go to my old friends: Jess, Peter, Déric, Félix, and Maxime.

Enfin, j'aimerais adresser quelques mots en français à la femme qui m'accompagne et me supporte depuis les sept dernières années. Merci Audrey pour ton soutien, ta patience et présence: je t'aime et n'y serais jamais arrivé sans toi.

RÉSUMÉ

Les semiconducteurs à base d'oxydes de métaux nanostructurés sont des matériaux dont l'étude est largement répandue dans le domaine des applications solaires, tel que le démontre l'engouement pour les cellules solaires de type Grätzel. L'oxyde de tungstène (WO_3) est un matériau qui a des propriétés électrochromiques et possède une énergie de bande ≈ 2.5 eV, ce qui lui a permis d'être étudié dans des applications reliées à la conversion (photocatalyse ou photoélectrochimie) de l'énergie solaire. Cependant, la valeur de l'énergie de bande du WO_3 est telle qu'il est transparent pour une grande partie du spectre solaire, ce qui limite l'efficacité de conversion de puissance des dispositifs à base de WO_3.

Les matériaux à conversion ascendante de photons sont des matériaux qui peuvent absorber plusieurs photons de faible énergie et émettre un photon de haute énergie. Notamment, les nanoparticules à conversion ascendante de photons sont grandement étudiées pour leur capacité à tranformer deux ou plusieurs photons infrarouge en un photon visible, dans des domaines tels que les applications biomédicales et de l'énergie solaire. En ce qui a trait aux applications en énergie solaire, une partie importante du spectre solaire est composée d'infrarouge, donc de photons qui ont une énergie trop faible pour générer une paire électron-trou dans un semiconducteur à large bande interdite, tel que le WO_3. Les nanoparticules à conversion ascendante de photons sont donc d'intéressantes candidates pour transformer la lumière infrarouge en lumière qui puisse être utilisée par des semiconducteur à grande énergie de bande, tels que les oxydes de métaux.

Ce projet de maîtrise consiste à ajouter des nanoparticules à conversion ascendante de photons ($NaGdF_4$:Er^{3+}, Yb^{3+}) à un oxyde de métal nanostructuré, à savoir le WO_3. De cette façon, l'objectif est d'augmenter l'efficacité de conversion de puissance du WO_3 lorsqu'exposé à la lumière solaire. L'intégration des deux nanomatériaux est motivée par le contact intime qui peut s'établir entre eux, dans le but de potentiellement optimiser leur interaction.

L'article 1 inclus dans le mémoire concerne des nanoparticules de $NaGdF_4$:Er^{3+}, Yb^{3+} mélangées à du WO_3 en phase liquide pour le dépôt de couches minces nanocomposites sur un substrat composé d'une paire d'électrodes faite de verre conducteur (ITO). Après avoir optimisé les paramètres de préparation et de dépôt des couches minces, ces dernières ont été systématiquement caractérisées. La morphologie a été étudiée à l'aide de la microscopie à force atomique, la structure à l'aide de la diffraction de rayons-X, les propriétés de photoluminescence à l'aide d'un microscope hyperspectral à fluorescence et les propriétés électriques par des mesures de courant en fonction du temps sous irradiation infrarouge. Principalement, nous observons

une augmentation du courant dans les couches minces composées de $NaGdF_4$:Er^{3+}, Yb^{3+} et WO_3 lorsqu'elles sont exposées à de la lumière infrarouge par rapport au courant dans le noir, ce qui est attribué à la production d'un photocourant. Nous émettons l'hypothèse que les photons émis par le laser à 980 nm sont probablement absorbés par les nanoparticules à conversion ascendante de photons et convertis en lumière visible qui peut être collectée par le WO_3, générant ainsi un photocourant.

ABSTRACT

Nanostructured metal oxides semiconductors are widely used in solar energy related applications, such as in dye-sensitized solar cells. Tungsten trioxide (WO_3) is an electrochromic material, extensively investigated in solar energy conversion (e.g. photoelectrochemistry) and conservation (e.g. electrochromism). However, WO_3, because of its wide bandgap (≈ 2.5 eV), is transparent to an important portion of the solar spectrum and can effectively absorb light only up to ca. 500 nm, which limits the power conversion efficiency of devices based thereon.

Upconverting materials can absorb several low-energy photons to emit one high-energy photon. In particular, upconverting nanoparticles are widely studied in biomedical and solar energy applications, as they can transform two or several infrared photons in a visible photon. As the Sun contains important NIR and IR portion, UCNPs are interesting candidates to transform NIR or IR light into visible light to be absorbed by wide bandgap semiconductor, such as metal oxides.

The work presented in this master's thesis consists in embedding $NaGdF_4$:Er^{3+}, Yb^{3+} UCNPs into a nanostructured WO_3 matrix. The objective is to increase the power conversion efficiency of WO_3 after solar light harvesting. The integration of two materials with nanostructured nature has the potential to lead to a good synergy between them.

We include an article in this master's thesis. In this article, we report on the mixing of $NaGdF_4$:Er^{3+}, Yb^{3+} UCNPs with WO_3 in solution and on the deposition of the two-component solution on ITO-patterned electrodes. After engineering the fabrication and deposition of the thin nanocomposite films, they were systematically studied. Morphology was studied by atomic force microscopy, structure by X-ray diffraction, photoluminescence by fluorescence hyperspectral microscopy, and charge carrier transport under NIR irradiation by current-time measurements. Notably, we observed an increase in the value of the current with respect to the dark current when UCNP/WO_3 thin films were exposed to 980 nm continuous laser irradiation. This increase in the value of the current is tentatively attributed to the absorption of the NIR light by the UCNPs, which is upconverted into visible light to be harvested by the WO_3, eventually generating a photocurrent.

TABLE OF CONTENTS

DEDICATION iii

ACKNOWLEDGMENTS iv

RÉSUMÉ v

ABSTRACT vii

TABLE OF CONTENTS viii

LIST OF FIGURES xi

LIST OF ACRONYMS AND ABBREVIATIONS xv

LIST OF APPENDICES xvi

CHAPTER 1 INTRODUCTION AND LITERATURE REVIEW 1

1.1 Solar energy conversion 1

1.1.1 Solar cells 3

1.1.2 Beyond Shockley–Queisser limit 5

1.1.3 Metal oxides in solar energy conversion 7

1.1.3.1 TiO_2: a paradigmatic example 7

1.1.3.2 WO_3 8

1.1.4 Upconversion process as a strategy to photosensitize metal oxides . . 9

1.1.4.1 Upconversion: origin and mechanisms 9

1.1.4.2 Synthesis of UCNPs 11

1.1.4.3 Internal quantum yield of lanthanide-based UCNPs 12

1.1.4.4 Application of UCNPs to solar cells 13

1.2 Problem definition 14

1.3 Objective of the work 15

1.4 Plan of the thesis 15

CHAPTER 2 EXPERIMENTAL SECTION 16

2.1 Materials 16

2.1.1 WO_3 synthesis 16

2.1.2 Upconverting nanoparticles synthesis 16

2.1.3 Fabrication of the thin films . . . 18
2.2 Microfabrication of the electrodes . . . 18
2.2.1 General remarks . . . 18
2.2.2 Microfabrication process . . . 19
2.3 Characterization . . . 21
2.3.1 Photoluminescence properties of UCNPs . . . 21
2.3.2 X-ray diffraction . . . 22
2.3.3 Atomic force microscopy . . . 22
2.3.4 Electrical measurements in dark and light conditions . . . 24

CHAPTER 3 ARTICLE 1: TOWARDS NEAR-INFRARED PHOTOSENSITIZATION OF TUNGSTEN TRIOXIDE NANOSTRUCTURED FILMS BY UPCONVERTING NANOPARTICLES . . . 25
3.1 Authors . . . 25
3.2 Abstract . . . 25
3.3 Introduction . . . 26
3.4 Experimental section . . . 27
3.4.1 Microfabrication of the electrodes . . . 27
3.4.2 Materials and fabrication of the thin films . . . 27
3.4.3 Characterization . . . 28
3.5 Results and discussion . . . 29
3.5.1 Thin film preparation and characterization . . . 29
3.5.2 Electrical Measurements . . . 33
3.6 Conclusions and perspectives . . . 35
3.7 Acknowledgements . . . 35
3.8 Supplementary information to article 1 . . . 36
3.8.1 Authors . . . 36
3.8.2 Supplementary information . . . 36

CHAPTER 4 COMPLEMENTARY RESULTS . . . 39
4.1 Choice of the configuration . . . 39
4.2 Effect of the thermal treatment temperature on UCNPs photoluminescence properties . . . 40
4.3 Effect of the UCNPs size . . . 41
4.4 Towards a better understanding of the results presented in article 1 . . . 43
4.4.1 Current-time measurements of 8 mol % UCNP/WO_3 thin films under white light . . . 43

4.4.2 Current-time measurements of 8 mol % UCNP/WO_3 thin films under chopped light at variable frequency 44
4.4.3 Temperature-dependent current-time measurements of 8 mol % UCNP/WO_3 thin films under chopped light 45
4.5 Results on $LiYF_4$: Tm^{3+}, Yb^{3+} UCNPs 46

CHAPTER 5 GENERAL DISCUSSION 49

CHAPTER 6 CONCLUSIONS AND PERSPECTIVES 51
6.1 Conclusions 51
6.2 Perspectives 52

BIBLIOGRAPHY 53

APPENDICES 63

LIST OF FIGURES

Figure 1.1 Spectral distribution of Sun's irradiation [1]. 2

Figure 1.2 Bandgap structure of a semiconductor. The bandgap energy (E_g) corresponds to the energy difference between the edges of the conduction(E_c) and valence band (E_v). 3

Figure 1.3 a) Losses mechanisms inside a solar cell [2]: (1) Thermalization, (2) Opical transparency, (3) Electron hole recombination, (4) Loss at the p-n junction and (5) Contact losses. b) Maximum achievable power conversion efficiency vs bandgap energy in SQ scenario [3]. 6

Figure 1.4 Diagram for the three major mechanisms by which upconversion may occur. Reproduced from [2]. 11

Figure 1.5 Lumiscence measurement setup to evaluate the efficiency of UC materials. Reproduced from [4]. 12

Figure 2.1 Process flow of the synthesis of WO_3. In the first step, an aqueous solution of Na_2WO_4 is passed through a proton-exchange resin. Then, H_2WO_4 is collected in ethanol. After the evaporation of the solvent, an organic stabilizer (PEG-200) is added. As prepared sols could be used within 72 h. 17

Figure 2.2 Illustration of the synthesis of UCNPs. After the preparation of the precursors, lanthanides trifluoroacetates are injected in oleic acid and octadecene at 315°C, before aging for 1 h at constant temperature. Image produced by Dr. Marta Quintanilla. Printed with permission from the creator. 18

Figure 2.3 AFM topographical image of ITO substrate, as purchased from Colorado Concept Coating. Root mean square roughness (R_{RMS}) is about 5.4 nm (area is 2×2 μm). 19

Figure 2.4 Optical microscope image of the patterned electrodes prior to the chemical wet etching step. 20

Figure 2.5 Microfabrication steps for planar ITO-patterned electrodes. 21

Figure 2.6 AFM working principle. A sample is placed under a silicon tip attached to a cantilever. Depending on the operating mode, the tip can be in contact or touch the sample intermittently. The deflection of the cantilever allows to obtain information on the topography of the sample investigated. Reproduced from [5]. 23

Figure 2.7 Comparison of the two operating modes. In contact mode, the sample and the tip are in contact, and the deflection of the cantilever is proportionnal to the forces acting on the tip. In tapping mode, the tip oscillates near the surface at a given frequency, resulting in a change of the amplitude of oscillation and force between the tip and the sample. 23

Figure 2.8 Setup for the electrical measurements. WO_3 or UCNP/WO_3 thin films were deposited on patterned substrates. A constant bias was applied, and the current was measured over time. 24

Figure 3.1 (a) TEM image of β-$NaGdF_4$:Er^{3+}, Yb^{3+} UCNPs. (b) Experimental configuration adopted for the electrical characterization (photocurrent vs time). Topographical AFM images of (c) WO_3 and (d) 8 mol% UCNP/WO_3 films, deposited on glass, treated at 385°C. (e) PL spectrum of β-$NaGdF_4$:Er^{3+}, Yb^{3+} UCNPs drop-cast on glass and thermally treated at 385°C (right y axis) and optical transmission spectrum of a WO_3 film ($\approx$1 μm in thickness), deposited on glass and thermally treated at 385°C (right y axis). Inset figure 3.1(e): PL spectrum of the UCNPs, drop-cast on glass and dried at room temperature. 31

Figure 3.2 XRD patterns of β-UCNPs, 45 nm in diameter, drop-cast on glass. After room temperature drying and thermal treatment at 385°C, UCNPs are in the β-phase (hexagonal phase, patterns 1 and 2). The peak positions for the α and β phases are included at the bottom of the figure [6]. 32

Figure 3.3 Current-time measurements under NIR chopped light (60 s in the dark and 30 s under irradiation, λ_{exc}=980 nm, power density=1 W/cm^2) for films deposited on patterned ITO with an interelectrode distance of 100 μm and thermally treated at 385°C made of (a) 8 mol% UCNP/WO_3 and (b) WO_3 (see figure 3.7). Samples were kept under constant electrical bias for 300 s in ambient light conditions, followed by 300 s in the dark, before chopping the light. 34

Figure 3.4 Optical microscope images of 16 mol% UCNP/WO_3 films thermally treated at 385°C deposited on a) glass substrate and b) SiO_2. 36

Figure 3.5 Partial $NaGdF_4$:Er^{3+}, Yb^{3+} UCNPs energy levels diagram.For the sake of clarity, only the energy levels involved in the upconversion process are shown. Dashed lines are associated to energy absorption, dotted lines are associated to energy transfer, full grey lines are associated to non-radiative processes, and full double lines are associated to radiative processes. 37

Figure 3.6 XRD measurements of WO_3 (pattern 1) and 8 mol % UCNP/WO_3 thin films deposited on glass substrate and thermally treated at 385°C (pattern 2). 37

Figure 3.7 Current-time measurements of pure WO_3 thin films thermally treated at 385°C deposited on patterned ITO with an interelectrode distance of 100 μm under LED white light (Thorlabs, model LIU004). Initially the sample was kept in dark conditions for 300 s at an applied electrical bias of 1 V, followed by 300 s under LED white light, followed by dark conditions. 38

Figure 4.1 Two configurations investigated at the beginning of the project. a) "Layered" configuration: the UCNPs are deposited on a WO_3 thin film. b) "Nanocomposite" configuration: the UCNPs are embedded in the WO_3. 39

Figure 4.2 PL properties of a) hexagonal b) cubic phase UCNPs deposited on WO_3 (full lines). The PL properties of a thin film made from pure UCNPs (dashed lines), drop-cast on a glass substrate are also shown for reference. 40

Figure 4.3 PL intensity of pure hexagonal UCNPs treated at different temperatures. Size of the UCNPs is 35 nm. UCNPs dispersed in water were drop-cast on a glass substrate and thermally treated at RT, 400°C, and 550°C. Green emission is strongly affected by the temperature of the thermal treatment. 41

Figure 4.4 Current-time measurements of thin film samples deposited on substrates patterned with ITO electrodes and thermally treated at 400°C. The samples were kept under electrical bias (V=0.7 V) for 5 min in ambient light conditions followed by 5 minutes in the dark before chopping the light (λ_{exc}=980 nm). Nanocomposite films containing 8 mol %UCNPs/WO_3 with (A) 35 nm-sized hexagonal UCNPs and (B) 95 nm-sized hexagonal UCNPs. 42

Figure 4.5 Current-time measurements of UCNP/WO_3 (8 mol %) thin films thermally treated at 385 °C deposited on patterned ITO with an interelectrode distance of 100 μm under white LED light (Thorlabs, model LIU004). Samples were kept under constant electrical bias (1 V) for 300 s in dark conditions, followed by 300 s under white LED light, followed by dark conditions. An increase in current is observed when the white LED is shed on the sample. 43

Figure 4.6 Current-time measurements under NIR chopped light for ≈ 8 mol % UCNP/WO_3. Thin films were deposited on patterned ITO with an interelectrode distance of 100 μm and thermally treated at 385°C. Samples were kept under constant electrical bias for 300 s in ambient light conditions, followed by 300 s in the dark. Frequency of chopping light was 1 Hz and 0.5 Hz, respectively. 44

Figure 4.7 a) Temperature-dependent current-time measurements under NIR chopped light (λ_{exc}=980 nm, power density ≈ 5 W/cm^2) for 8 mol % UCNP/WO_3. Thin films were deposited on patterned ITO with an interelectrode distance of 100 μm and thermally treated at 385°C. b) Table showing the evolution of the substrate temperature and the on/off ratio R. Temperature-dependent current-time measurements at c) T_1=50°C, d) T_2=45°C, e) T_3=40°C and f) T_4=35°C. 46

Figure 4.8 TEM image of $LiYF_4$: Tm^{3+}, Yb^{3+} UCNPs. This image was collected by Dr. Marta Quintanilla (INRS-EMT, Prof. F. Vetrone's research group). 47

Figure 4.9 Photoluminescence properties of $LiYF_4$: Tm^{3+}, Yb^{3+} UCNPs, drop-cast on a glass substrate and dried at RT. 47

Figure 4.10 XRD pattern of the $LiYF_4$: Tm^{3+}, Yb^{3+} powder. The peaks are indexed to the hexagonal phase [6]. This measurement was performed by Dr. Marta Quintanilla (INRS-EMT, Prof. F. Vetrone's research group). 48

Figure 4.11 Current-time measurements under NIR chopped light (λ_{exc}=980 nm, power density ≈1 W/cm^2) of $LiYF_4$: Tm^{3+}, Yb^{3+}/WO_3 thin films deposited on patterned ITO electrodes (L = 100μm) and thermally treated at 385°C. 48

LIST OF ACRONYMS AND ABBREVIATIONS

AFM	Atomic Force Microscopy
a-Si	Amorphous Silicon
c-Si	Crystalline Silicon
CW	Contiuous Wave
DSSCs	Dye-Sensitized Solar Cells
E_c	Conduction band energy level
E_g	Bandgap energy
ESA	Excited State Absorption
ETU	Energy Transfer Upconversion
E_v	Valence band energy level
eV	Electronvolt
IR	Infrared
IPA	Isopropyl Alcohol
ITO	Indium Tin Oxide
η	Power Efficiency
NIR	Near-infrared
PA	Photon Avalanche
PARISS	Prism And Reflector Imaging Spectroscopy System
$P_{density}$	Power density
PL	Photoluminescence
PV	Photovoltaics
QY	Quantum Yield
TEM	Transmission Electron Microscopy
TW	Terawatts
UC	Upconversion
UCNPs	Upconverting Nanoparticles
V_{OC}	Open-circuit Voltage
XRD	X-ray Diffraction

LIST OF APPENDICES

Appendix A Theoretical estimation of the photocurrent generated in 8 mol % $NaGdF_4$: Er^{3+}, Yb^{3+} UCNP/WO_3 thin films 63

CHAPTER 1 INTRODUCTION AND LITERATURE REVIEW

The discovery of the photovoltaic effect is attributed to Edmond Becquerel, the French scientist who studied the effect of light on electrolytic cells. He observed an electric current between two platinum electrodes covered by photosensitive materials, such as AgCl or AgBr, immersed in an acidic solution (such as dilute sulfuric acid) when one electrode was irradiated by solar light [7]. It took about a century to reach the development and production of devices that convert light into electricity of any technological interest from the viewpoint of energy conversion efficiency. This improvment in the efficiency was stimulated by the space programs of the 1960s, and above all by the energy crisis of the 1970s [8].

In 2010, the global energy consumption was about 10 terawatts (TW), and recent estimations claim that, by 2050, approximately 30 TW of energy will be required annually to fulfill human-related activities [9]. Among other possibilities, solar energy has the potential to meet this requirement. Indeed, solar power arriving at Earth's surface is about 120 000 TW, which is approximately 10 000 times more that we actually need [10]. However, to meet the never stopping increase in energy demand, it is mandatory to have technologies that permit to produce highly efficient solar cells. In order to reach the efficiency required for satisfying the energy demand, numerous challenges are still to be addressed.

The Sun is a star that emits light with an extended range of wavelengths that can be approximated by a blackbody at a temperature of about 5800 K, which emits from the ultraviolet (UV) to the visible (VIS) and the infrared (IR), with a maximum located around 500 nm. However, the atmosphere protecting the Earth affects the spectral emission of the sun: the UV is partly absorbed by the ozone, H_2O absorbs the emission at about 900, 1100, 1400, 1900 nm, and CO_2 absorbs at about 1800 and 2600 nm. The position of the Sun also has an effect on terrestrial irradiation, accounted by the air mass (AM) coefficient, which represents the optical path length of Sun's irradiation. It can be approximated by AM$\approx 1/\cos\phi$, where ϕ is the angle of elevation of the Sun with respect to the normal to the Earth's surface. The standard Sun's spectrum is named AM1.5 ($\phi = 48.2°$) [11]. The spectrum of the light that irradiates the Earth's surface is presented on figure 1.1 [1].

1.1 Solar energy conversion

Now that we know what Sun's irradiation looks like on Earth's surface, we can try to figure out how we can use this incoming light. The absorption of photons that results in the

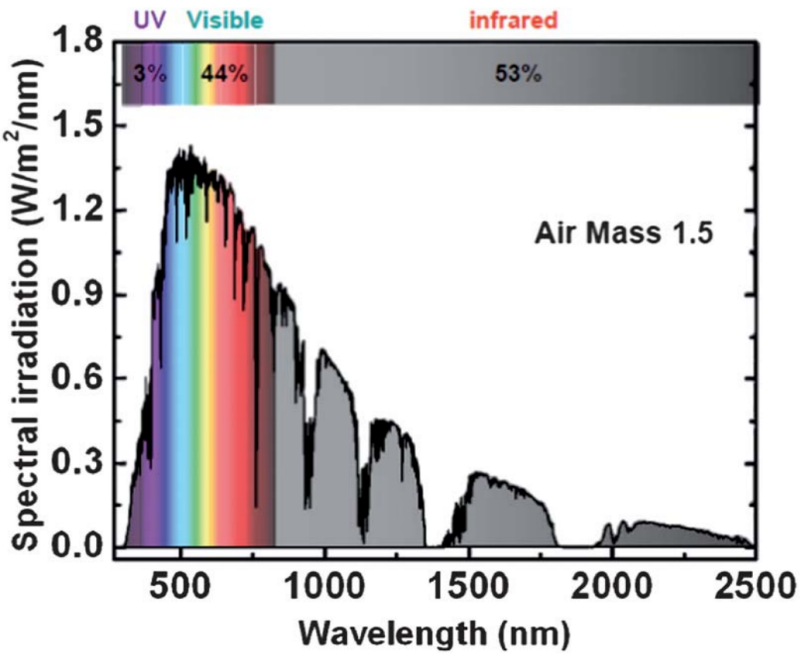

Figure 1.1 Spectral distribution of Sun's irradiation [1].

generation of charge carriers can take place in semiconductor materials. An important characteristic of semiconductors is the bandgap, namely the difference in energy between the edges of the valence and conduction bands. Figure 1.2 shows the band structure of a typical semiconductor. It is composed of a valence band whose top edge is associated to the energy E_v, and a conduction band, whose bottom edge is located at the energy E_c. The valence band is usually filled with electrons, so as the electrons cannot significantly move into the material, while the conduction band is empty. The energy difference between the valence and conduction band edges is the bandgap (E_g) and is expressed by equation 1.1:

$$E_g = E_c - E_v \tag{1.1}$$

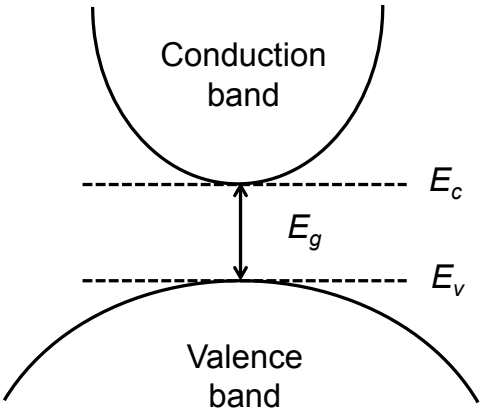

Figure 1.2 Bandgap structure of a semiconductor. The bandgap energy (E_g) corresponds to the energy difference between the edges of the conduction(E_c) and valence band (E_v).

When a photon hits a semiconducting material, one of the following situations occurs:

1. The photon is absorbed by the semiconductor, and an electron-hole pair is generated;
2. The photon is transmitted by the material. In this case, the semiconductor is "transparent" to the photon;
3. The photon is reflected by the surface of the semiconductor.

In the first situation, the energy of the incoming photon has to be at least E_g. As a result, an electron is liberated from its bound state and is promoted to the conduction band, such as it can move and contribute to the current. When an electron is promoted to the conduction band, it leaves an 'empty space' behind. This space is an absence of electron, and can therefore be seen as a particle with a positive charge (hole) that can move within the material [12].

In the second situation, the energy of the incoming photon cannot be effectively used by the semiconductor to generate charge carriers. Several approaches are feasible to improve the light harvesting properties of a semiconductor: some of them are presented in section 1.1.4.

An anti-reflection coating is normally placed on top of PV device in order to avoid the third situation, namely the reflection of the incoming light on the material.

1.1.1 Solar cells

The first class of solar cells investigated during the 1960s were based on III-V (e.g. GaAs [13]) or II-IV semiconductors (e.g. CdTe [14]). Around the same time, the possibility to produce

polycrystalline in industrial quantity came up. As a result of more than 50 years of research and development in the field on silicon-based technologies, the cost of production of energy produced by silicon-based solar cells is now low (ca 3 $/W), and the power conversion efficiency high (about 25 % for c-Si) [11]. This class of solar cells, exclusively based on c-Si, is referred as 'first generation' solar cells. It relies on a p-n junction, which is an interface between an n-type (large electrons concentration) and a p-type (large hole concentration) semiconductor (as indicated on figure 1.3 a)). Second generation solar cells are based on thin films technology and use, among others, amorphous silicon (a-Si) or CdTe. They are less efficient than c-Si solar cells, but the advantage of such solar cells is the relatively low cost and the possibility to use a wide range of substrates, such as flexible substrates [15].

In the field of solar energy conversion, the power conversion efficiency η is the ratio of the power that can be extracted from the solar cell to the power irradiating the solar cell, namely:

$$\eta = \frac{P_{out}}{P_{in}} \tag{1.2}$$

There are many factors affecting the final efficiency of a solar cell, but the two major power-loss mechanisms in a single-junction solar cell are the inability to absorb photons with energy lower than the bandgap and the thermalization of photons with energy higher than the bandgap. When combined, these two effects are responsible for about 50% of the losses [2].

The two first generations of solar cells are based on a single p-n junction and subject to the Shockley-Queisser (SQ) limit, which is a thermodynamic efficiency limit that is related to the value of the bandgap of the semiconductor [3]. The SQ limit relies on several assumptions. First, when a photon with an energy higher than E_g is absorbed by the semiconductor, the excess of energy is transformed into heat, which creates phonons. Then, every electron and hole that do not recombine diffuse to their respective electrodes to be eventually extracted. The only allowed recombination mechanism takes place via radiative process. Also, it is supposed that the photoactive material is thick enough to harvest as much light as possible at a certain wavelenght. It was also assumed that the Sun is a blackbody at 6000 K, that one photon generates one electron-hole pair, and that photons with energy below the bandgap do not generate an electron-hole pair. The calculations of the theoretical maximum power that can be extracted from a single p-n junction lead to the two following conclusions [3]:

1. The optimal bandgap is located for a single-junction solar cell at around 1.2 eV;
2. The highest efficiency attainable for a device based on a material with $E_g = 1.2$ eV is about 30%.

These two conclusions are also illustrated on figure 1.3 b).

It is now appropriate to present what is called 'third generation photovoltaics'. The goal of third generation PV is to overcome the Shockley–Queisser limit, preferably at low cost. A broad range of possibilities has been proposed to overcome this limit, and every possibility aims at either changing the design of the solar cell or the light harvested by the solar cells. Third generation PV is still at a research level, and is not ready yet for commercialization. The next section will illustrate how it is possible to overcome the limit inherent to single junction solar cells.

1.1.2 Beyond Shockley–Queisser limit

Among the many feasible possibilities aiming at attaining solar cells with power conversion efficiency higher than the SQ limit, four categories can be identified, namely: multi-junction cells, intermediate-band cells, hot carrier cells and spectrum conversion [15].

Multi-junction cells or 'multiple energy level approach' refers to the possibility of using several energy gaps to absorb different wavelengths and portions of the solar spectrum. This approach was first proposed by Jackson in 1995, and it consists in stacking p-n junctions with different materials (i.e. with different bandgaps), such as the material with the highest bandgap absorbs first the light [16]. Being transparent to higher wavelenghts, the rest of the light is absorbed by subsequent p-n junctions with lower bandgaps [17]. They can be monolithically integrated, i.e. made from several layers put in mechanical and electrical contact, but preparation of such devices is challenging, because the electrical characteristics of each layer have to be matched, without what electrons can be absorbed by a layer without being collected. Four-junction solar cells are to this day the devices with the highest efficency reported (ca. 46%, measured at a concentration of 508 suns, Fraunhofer, 2014).

The second approach presented is the 'intermediate-band cells'. This strategy consists in introducing at least one energy level within the bandgap of the photoactive material, e.g. by incorporating an impurity. Historically, the first two examples reported in the literature are the addition of B in SiC and In in Si [18, 19]. However, the addition of impurities in a solar cell also increases the probability of radiative and nonradiative recombination. If this approach appears interesting in theory, no experimental work has shown that it could indeed increase the efficiency of the solar cell [18].

The third approach is based on the idea of using 'hot carriers', i.e. carriers generated by a photon with an energy higher than E_g. It was proposed in 1982 by Ross and Nozik [20]. Usually, in solar cells, an incoming photon with energy greater than the bandgap generates

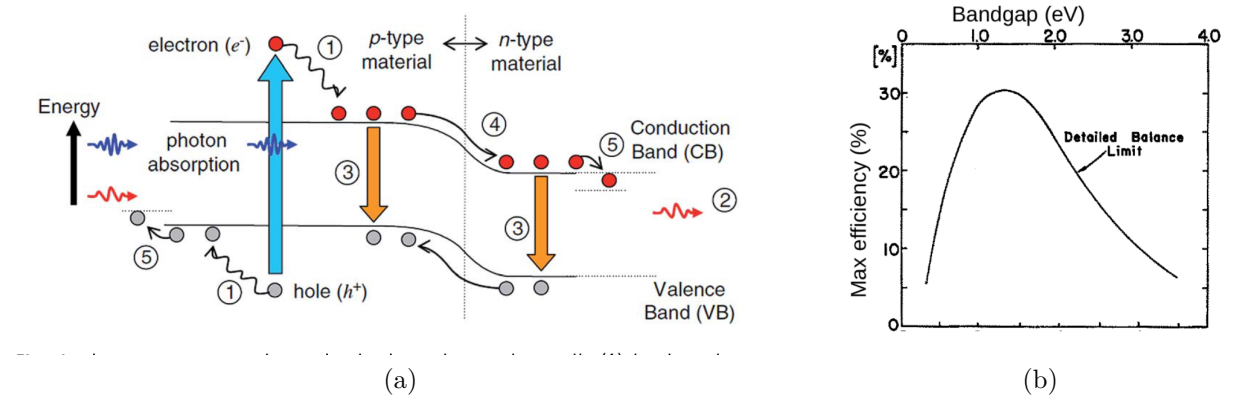

(a) (b)

Figure 1.3 a) Losses mechanisms inside a solar cell [2]: (1) Thermalization, (2) Opical transparency, (3) Electron hole recombination, (4) Loss at the p-n junction and (5) Contact losses. b) Maximum achievable power conversion efficiency vs bandgap energy in SQ scenario [3].

an electron-hole pair whose energy can be higher than the bandgap energy [15]. After a relative small amount of time ($\leq$ 1 ps), the hot carriers will relax, thus transferring their excess of energy to the lattice of the semiconductor, which results in the production of optical phonons, namely oscillation of the lattice resulting in a vibrating motion. These phonons will interact with other phonons, and the energy in excess of the bandgap will be simply lost. The major concept behind this approach consists in slowing down (>> ps) the transformation of the extra energy of the photogenerated carriers into phonons, such as these hot carriers could be collected. However, experimental implementations of this idea is somehow limited, and much of the work has been made from a computational point of view. In this perspective, theoretical calculations estimated that efficiencies of about 80 % are attainable in solar cells usings hot carriers and concentrated sunlight [21]. One instance of this general approach is called 'multiple carrier excitation'. It also relies on the use of carriers generated from high-energy photons ($E_{h\nu} \geq E_g$). The mechanism involved in this process is still not completly understood, but it is believed that carriers generated with high-energy photon can undergo impact ionization, which allows creating several electron-hole pairs [15]. To this day, the most efficient system in which this phenomenon occurs is based on quantum dots (QDs), where up to seven electron-hole pairs can be created by the absorption of one photon. It has been shown in PbSe QDs, but also in II-VI semiconductors and silicon-based QDs [22, 23].

The last approach herein presented, namely the spectrum conversion, consists in modulating the incoming light. The main goal of this approach is to make a better use of Sun's spectrum by transforming the incoming light such as it becomes usable by the semiconductor material. Several optical processes can be used, the most relevant being: quantum cutting (QC),

down-shifting (DS), and upconversion (UC). Quantum-cutting refers to the process where a material absorbs one high energy photon and re-emits two (or more) low energy photons. Down-shifting is an optical process where one high-energy photon is absorbed by a material, that after non-radiative relaxation, emits one photon having a fraction of the energy of the initial photon. A brief overview on QC and DS fundamental aspects and applications can be found in [24]. In the UC process, two (or more) low energy photons are subsequently absorbed by a material that can then emit a photon with higher energy [25]. The use of the UC process definitely fits into the 'third generation' solar cells approach: fundamental considerations and applications in PV devices will be presented in section 1.1.4.

1.1.3 Metal oxides in solar energy conversion

The aim of this section is to present how metal oxides have been used in solar energy conversion. One of the most cited examples is the use of metal oxides in dye-sensitized solar cells (DSSCs)[1]. DSSCs are based on a dye-coated semiconductor (e.g. TiO_2) and an electrolyte sandwiched between two transparent electrodes. The seminal work published by O'Reagan and Grätzel showed that it was possible to attain 7 % efficiency in a DSSC [29]. Since then, a considerable amount of work have been made towards the development of DSSCs with high efficiency. For the sake of clarity and concision, we will not explain with great details the working principle of DSSC and will rather focus on semiconductors used in these cells, more specifically nanostructured metal oxides [29]. This example of solar cells shows advantages over the classic p-n junction, such as: their convenient synthesis route, low cost, thermal stability and tunability.

1.1.3.1 TiO_2: a paradigmatic example

The idea of photosensitizing a material with a relatively wide bandgap dates back in the 1970s, and scientists were at that time motivated by the investigation of photoelectrochemical processes [30]. In the 1970s, photoelectrochemical devices based on metal oxide photoelectrodes (e.g. ZnO) had an efficiency of ca. 1%, and the first use of dye-sensitized nanostructured TiO_2 in photoelectrochemical devices was reported by Deb in 1978 [30, 31, 32]. Then, the research slowly moved towards the use of semiconductors with narrow bandgap such as Si. The key behind the finding made by O'Reagan and Grätzel that prompted renewed interest in the DSSCs approach was the use of *mesoporous* metal oxides electrodes, i.e. metal oxides

[1]Metal oxides are also used in other solar energy conversion devices, such as quantum-dots and organic solar cells. For the sake of concision and clarity, we will not discuss these approaches, but these topics are covered in [26, 27] (for QDs solar cells) and [28] (for organic solar cells).

containing nanometric size pores. Notably, the surface area of mesoporous metal oxides is estimated to be 1000 times higher than a bulk thin film. As a result, there is a better interaction between the dye and the semiconductor, which enhances the light harvesting properties of the cells.

TiO_2 is a stable metal oxide that is widely used in a broad range of applications, such as pigment or sunscreen. It can exist in several crystal structures, such as the anastase and rutile structures. Most of the research done during the last twenty years aimed at developing different synthesis routes and nanostructures (e.g. nanoparticles, nanowires). It can be produced by several ways, such as sol-gel, hydrothermal, chemical vapor deposition, physical deposition and electrodeposition [33]. Among others, the enhancement of the charge carrier transport properties, and the minimization of charge recombination have been widely investigated in TiO_2. TiO_2 is still, to this day, the semiconductor that is mostly used to produce nanostructured electrodes for DSSCs.

1.1.3.2 WO_3

In this section the emphasis will be put on WO_3, a semiconductor with a large bandgap (ca 2.5 eV). The bandgap of this material is more suitable than TiO_2 ($E_g \approx 3.2$ eV) from the solar light application point of view. Indeed, unlike TiO_2 that absorbs only in the UV region of the solar spectrum, WO_3 can absorb wavelenght up to 500 nm [34]. Apart from its bandgap, WO_3 has many interesting features for technological applications. It can indeed be obtained in various crystalline structures, nanostructured, mesoporous, transparent to a large portion of the solar spectrum and synthetized by many different synthesis routes, including sol-gel, hydrothermal, anodization methods, sputtering, chemical vapor deposition [35, 36].

This material is also widely studied for its electrochromism properties, which means that it can undergo a reversible change in color under electrical bias. Thanks to this property, WO_3 finds application in security devices and smart windows [37].

Several works have reported the use of solar energy conversion devices based on WO_3. For example, it has been used as hole blocking layer in OPV and photoanodes. As it is resistant against corrosion and can withstand aqueous acidic conditions, it has also been used for water splitting applications and photoelectrochemistry [38].

Recently, a lot of research has been going on to nanostructure WO_3, which could enhance the properties of the material. Among others, strategies consist in increasing the surface/volume ratio (which could result in a greater surface area for chemical reactions to take place) or reducing the size to benefit from quantum confinement effects [39].

1.1.4 Upconversion process as a strategy to photosensitize metal oxides

From what has been said in section 1.1.2, one possible way to go beyond Shockley-Queisser limit is to 'transform' the light before it reaches the material. In this section, the UC process is first presented from a theoretical point of view to illustrate why upconverting materials are interesting to photosensitize metal oxides.

1.1.4.1 Upconversion: origin and mechanisms

The origin of upconversion procress can be traced back in 1959, when Bloembergen proposed to make use of rare Earth salts in order to be able to detect infrared photons. As he pointed out, lanthanide-doped materials have a rich energy level diagram [40]. This phenomenon (upconversion) was then first observed by Auzel in 1966 [41]. There are two classes of materials in which upconversion can take place. First, UC process can take place in lanthanides or transition metal ions hosted in an inorganic material and, secondly, in organic chromophores [42]. As the work done for this thesis is stricly concerned with lanthanides-based UCNPs, the focus will be put on the mechanisms associated with this class of upconverting materials.

Lanthanides are 15 elements with $[Xe]6s^2 4f^n$ electronic configuration, where n represents the number of electrons in the $4f$ orbital, and $0 \leq n \leq 14$ [2]. The partial filling of the $4f$ orbital is responsible for the unique optical and magnetic properties of the lanthanides-based UCNPs. The completly filled $5s$ and $5p$ orbitals act as a shield, thus protecting the $4f$ orbital from the environment. These two characteristics explain why UCNPs exhibit sharp optical emission, and relatively long lifetime for their excited states (ranging from μs to ms) [43]. Since $4f^n$ transitions are Laporte-forbidden[2] in order to preserve the dipole moment, there is only a small probability of transition, which results in long excited state lifetime [44]. If n represents the number of electrons in $4f$ orbitals, there are $\frac{14}{n}$ possible electronic configurations: it explains the rich energy level diagram of lanthanides.

In particular, $NaGdF_4$:Er^{3+}, Yb^{3+} UCNPs are known to be one of the most efficient UC system (the ratio of the number of emitted photons to the number of absorbed photons varies from 0.005 % to 3 % depending on the size and crystalline phase of the UCNPs) and have been widely investigated [4, 45]. Their high efficiency can partly be explained by the choice of the host material. The fluoride host is a material of choice, because it has low lattice phonon energy, which considerably reduces the probability of non-radiative processes [46, 44]. Fluoride hosts are also very stable from a chemical viewpoint. The main

[2]Laporte selection rule states that electronic transitions that preserve parity are not allowed. It applies to atoms and molecules with an inversion center. Then, electronic transitions that conserve parity are unlikely to take place within centrosymmetric atoms and molecules.

features of the doping materials are the rich and ladder-like energy level diagram of Er^{3+} and the simple energy diagram of Yb^{3+}. Yb^{3+} only has two states: one ground state and one excited state [47]. In the case of $NaGdF_4$:Er^{3+}, Yb^{3+} UCNPs, the emission of light is the results of the interaction between two ions. Yb^{3+} with its high absorption cross-section and short lifetime absorbs the NIR photons and transfers them to Er^{3+}, that can absorb two low energy photons before emitting one high energy photon. Some of the limiting factors for efficient emission are the distance between the two emitting ions and the absorption cross-section [48]. $NaGdF_4$:Er^{3+}, Yb^{3+} UCNPs are interesting because they can easily be produced, and their size and phase can be tuned [44].

Upconversion may occur thanks to three working mechanisms: excited-state absorption (ESA), energy transfer upconversion (ETU), and photon avalanche (PA) (represented on figure 1.4) [44]. In the ESA mechanism, a single ion with ladder-like energy levels sequentially absorbs two (or more) photons to reach an excited state. Once in its excited state, a radiative process may occur. As seen on figure 1.4, a single ion absorbs a photon that is resonant with the energy gap between its ground (G) and excited state (E_1). After absorbing this photon, the ion is in its first excited state (E_1). Now, let us assume there exists a second excited state E_2, such that $E_1 - G = E_2 - E_1$. It means that if another photon is absorbed by the materials, the ion will be promotted to E_2, which could result in a radiative relaxation (from E_2 to G). In the cases where $E_1 - G \neq E_2 - E_1$, the ion has to be irradiate with several light sources with different wavelengths [45].

ETU requires that two types of ion, a sensitizer and an activator, are placed in proximity (few Å) in a host material [41]. This case has partly been introduced with the $NaGdF_4$: Er^{3+}, Yb^{3+} UNCPs. In this type of upconversion process, a photon with an energy resonant to the energy gap between the ground state and the excited state of the sensitizer (e.g. Yb^{3+}) is absorbed, which promotes the ion to its excited state. The same process occurs in another sensitizer. Then, a non-radiative energy takes place betwen the first sensitizer and the activator (e.g. Er^{3+}), which allows the activator to be promoted to its first excited state (E_1). Following this, the second sensitizer involved in this process transfers its energy to the activator, which promotes the activator from its first excited state to its second excited state (from E_1 to E_2). After the energy transfer, both sensitizer ions relax to their ground state, and the upconversion occurs from the E_2 level to the ground state of the ion [2]. A number of conditions have to be met in order for the upconversion to take place by ETU: the absorption cross-section of the sensitizer has to be high, the energy level spacing of the sensitizer and the activator has to be resonant, and the activator has to have 'long' life-time (normally ranges from 10 μs to 10 ms) [44]. As a rule of thumb, the ion concentration of the sensitizer is at least 10 times higher that the activator. ETU is often reported as the

most efficient process, and its main advantage over other optical processes (e.g. two-photon absorption) is the need of a low power laser source (as low as 1 W) [41].

PA is a mechanism that explains that upconversion can occur in a material above a threshold power of irradiation. Basically, it is a process where ESA process and cross-relaxation are both involved. The first excited state (E_1) of an ion is populated, followed by a resonant ESA that promotes the ion to E_2. Then, a cross-relaxation energy transfer takes places between this ion and another ion in its ground state, promoting the second ion to an excited state E_1. This energy is then transferred to the first ion, which populates its E_1 level. In the end, two ions are at level E_1, and one of them can absorb a photon and be promoted to E_2. Again, a cross-relaxation process can take place with another ion in the ground state, which results in three ions at E_1 level. By repeating these steps several times, the E_2 level of an ion can easily be populated, which results in a strong emission [2].

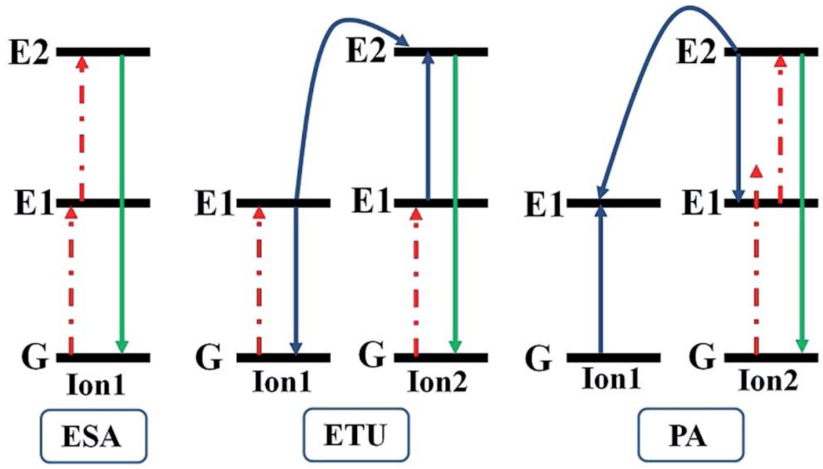

Figure 1.4 Diagram for the three major mechanisms by which upconversion may occur. Reproduced from [2].

1.1.4.2 Synthesis of UCNPs

UCNPs can be produced in many different ways, which allows to control, among others, their chemical composition, size, morphology, structure, and emissive properties. Many synthesis routes have been reported in the literature, such as: thermal decomposition, hydrothermal, co-precipitation, microwave-assisted, and ionic-liquid based synthesis [44]. As the synthesis of UCNPs is a field of research on its own, we will not give here a complete overview on the

topic [3]. The synthesis route adopted in the case of this master's thesis is based on a thermal decomposition process that will be presented in section 2.1.2.

1.1.4.3 Internal quantum yield of lanthanide-based UCNPs

A few works have been done on the characterization of the effficiency of UC materials [4, 49], which is accounted by the internal quantum yield (QY). QY is defined by equation 1.3 and corresponds to the ratio of the number of emitted (upconverted) photons over the number of photons absorbed by the UCNPs.

$$\text{Internal QY} = \frac{\#\text{photons emitted}}{\#\text{photons absorbed}} \tag{1.3}$$

The vast majority of the work published focus on lanthanide-based UCNPs. The first paper on systematic investigation of the QY of UCNPs was published by Boyer and van Veggel in 2010 [4]. They designed an experimental setup for measuring the QY of UCNPs using a spectrophotometer, an integrating sphere, and a continuous wave (cw) 980 nm laser diode. Using their setup, the authors were able to report that the QY of green emission in $NaYF_4$: Er^{3+}, Yb^{3+} is ranging from 0.005 % to 3 %, depending on the phase and the size of the nanoparticles. The experimental setup is shown on figure 1.5.

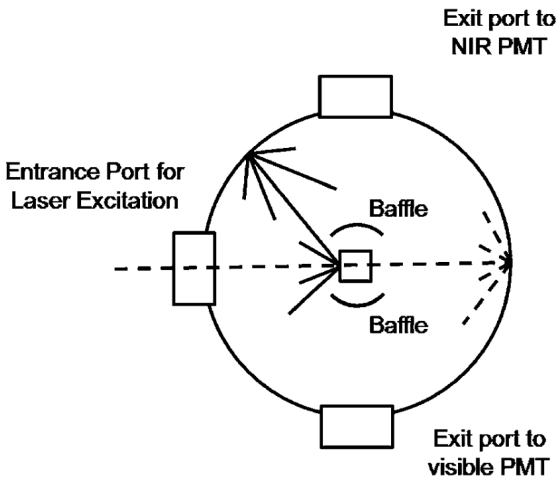

Figure 1.5 Lumiscence measurement setup to evaluate the efficiency of UC materials. Reproduced from [4].

[3] The reader interested by this topic should consult [44].

1.1.4.4 Application of UCNPs to solar cells

Even if UC materials have been extensively studied in the last decades, it took approximately thirthy years after the discovery made by Auzel before seeing the first application of UC materials in solar energy. More specifically, the first use of lanthanides ions for solar cells can be traced back to 1996, when Gibart et al. reported the use of a 100 μm-thick Er^{3+}/Yb^{3+} co-doped ceramic on the rear of a GaAs solar cell [50]. Before incorporating the co-doped ceramic layer in the solar cell, the authors were able to observe the UC green and red emissions attributed to Er^{3+} ion upon 891 nm illumination. They also observed that the response of the solar cell depends quadratically with the input power of the laser source, which supported that a two-photon process was taking place in their system. However, the authors concluded that the efficiency of GaAs solar cell at 891 nm (P_{density}= 25 W/cm^2) of about 2.5% was too low for any practical applications.

Trupke et al. were the first to publish a theoretical work on the possibility to improve solar cell efficiency by UC materials. Most notably, they reported on different geometries for c-Si solar cells and illumination conditions in order to show that the maximum efficiency attainable by UCNPs/c-Si is about 48% for non-concentrated light. This number increases up to 63.2 % for concentrated sunlight (about 46,000 suns) [51].

Historically, and following the development of well-established microelectronic processes and technologies, solar cells based on crystalline silicon were first extensively studied. It took almost ten years following the work made by Gilbart et al., for the community to start to use Er^{3+}-based UCNPs with crystalline silicon (c-Si) solar cell. The first example of this kind of work can be found in Shalav et al. [52]. In this pioneering work, they used $NaYF_4$: Er^{3+} UCNPs dispersed in a transparent acrylic medium that was attached to the rear of a bifacial c-Si cell. Under IR radiation (λ = 1523 nm, from a 5.1 mW laser), a quantum efficiency of 2.5% was reported. The work done by Liang et al. is an interesting example of a work using less conventionanal UC materials. The authors proposed to make use of $Gd_2(MoO_4)_3$: Er^{3+}. This nanophosphor is able, upon 1500 nm irradiation (power density $\approx$ 700 W/m^2), to emit light at 545, 665, 800, ans 980 nm, i.e. wavelengths that could be absorbed by crystalline silicon (E_g=1.1 eV or 1130 nm) [53].

Following the same historical pattern as in the solar cells field, UCNPs were subsequentlyused for amorphous silicon (a-Si) based solar cells. However, its larger bandgap compare to c-Si (1.75 vs. 1.1 eV) makes it more sensitive to transmission losses. The two first papers on the photosentization of a-Si solar cells by UCNPs were published by Wild et al [54, 55]. Indeed, they reported on the use of $NaYF_4$:Er^{3+}, Yb^{3+} in a thick transparent layer placed at the back of an a-Si solar cell. Upon irradiation at 980 nm (power $\approx$ 28 mW), they observed an

enhancement in current of about 6 %, which corresponds to an external quantum efficiency (the ratio of the number of charge carriers collected to the number of incident photons) of 0.03 % for the solar cell.

In 2010, the first work demonstrating the possibility to integrate UCNPs in DSSC solar cells was published by Shan and Demopoulos [56]. In this work, the authors synthesized 10 nm sized LaF_3: Er^{3+}, Yb^{3+} UCNPs to produce an upconverter/TiO_2 nanocomposite layer deposited on conducting glass (FTO) that was used as a working electrode. The overall efficiency of the solar cell under AM1.0 solar irradiation was about 2.7%, which was comparable to the efficiency of the solar cell without any UCNPs. This low efficiency was attributed to the inefficient absorption of the red upconverted light by the dye and the charge carrier recombination at the nanocomposite/electrolyte interface. Several papers have recently been published on the use of UCNPs in DSSCs [57, 58, 59, 60, 61]. Recently, several reviews have focused on the use of UCNPs in photovoltaics [62, 43, 63, 64].

1.2 Problem definition

Now that the theoretical background and the relevant literature on the topic have been sufficiently covered, it is possible to explicitly state the definition of the problem investigated during this project. First, this project makes use of a mesoporous, nanostructured solution-processed metal oxide, WO_3, that has been intensively studied in electrochromics as well as in solar energy conversion (photocatalysis and photoelectrochemistry). This material has a large bandgap of ca. 2.5 eV, which means that it is optically transparent for an important portion of the solar spectrum. It is clear that if one is interested to effectively use this material in solar energy conversion applications, it is necessary to extend its solar light absorption properties to NIR and IR portions of the solar spectrum. UCNPs are materials that can convert two (or several) low-energy photons into one high-energy photon. A possibility to overcome the limited spectral response of WO_3 could be the concomitant use of WO_3 and UCNPs. As seen in section 1.1.4, most of the work done in the field of using UC materials in solar cell consists in integrating a layer containing UCNPs on the rear face of the solar cells and to use a mirror to reflect the upconverted light back into the cell. The advantage of this approach is clear: in this fashion, it is possible to integrate the UC material without altering the design of commercially produced solar cells. Indeed, the addition of the UC layer only adds one step to the process, and the solar cells can be produced by the same industrial process. Using nanometric UC materials with nanostructured WO_3 could allow a better contact between the two materials, which could potentially increase the interaction between the two materials without the help of a mirror. Also, it could enable the possibility

to produce one layer containing metal oxide that is sensitive to the visible and NIR portions of the solar spectrum, thanks to the interaction between UCNPs and WO_3. Then, combining UCNPs with nanostructured WO_3 is an appealing approach to extend the spectral response of the semiconductor towards the NIR portion of the solar spectrum. It has been discussed in the previous section that nanostructured solution-processed metal oxides are interesting for many reasons. They are easy to produce in crystalline or amorphous forms, and are suitable for applications in photoelectrochemistry and electrochromism. In this context, lanthanide-based UCNPs can theoretically be used to photosensitize WO_3 in the NIR region of the solar spectrum.

1.3 Objective of the work

Our objective was to enhance the absorption properties of nanostructured solution-processed tungsten trioxide thin films to extend its light harvesting properties towards the NIR portion of the solar spectrum. This research question has been organised into three specific objectives that have been adressed in this master's thesis:

1. Develop a procedure that permits to synthesize thin films containing a known UCNPs/WO_3 ratio;
2. Characterize the uniformity and roughness of the thin films in order to assess their possible integration in solar energy conversion devices.
3. Evaluate the impact of the addition of UCNPs in WO_3 on the electrical photoresponse of WO_3;

1.4 Plan of the thesis

This master's thesis is separated in the following manner:

1. Chapter 2 presents the experimental techniques and methods used in this work;
2. Chapter 3 is the reproduction of an article submitted to *RSC Advances* in June 2015;
3. Chapter 4 contains complementary results, not included in the article, that are useful to a better understanding of the results;
4. Chapter 5 presents a general discussion;
5. Chapter 6 presents the conclusions and perspectives.

CHAPTER 2 EXPERIMENTAL SECTION

This chapter is separated into three sections. First, we describe how the materials were prepared. Then, we explain how the substrates where the materials are deposited were fabricated by microfabrication. Finally, we present the working principle of the experimental setup for the characterization methods.

2.1 Materials

In this first section, we present the synthesis routes of the materials under investigation (WO_3 and $NaGdF_4$:Er^{3+}, Yb^{3+} UCNPs). Then, we present how the thin films were fabricated.

2.1.1 WO_3 synthesis

WO_3 was prepared following a sol-gel synthesis reported in the literature [65]. Basically, Na_2WO_4 salt (Sigma Aldrich) was dissolved in water to obtain a solution of 0.5 M concentration and the obtained aqueous solution was passed through a proton-exchange resin (Dowex 50WX2, Sigma Aldrich). This resin has the property to substitute Na^+ with H^+ ion, such as H_2WO_4 solution can be collected. It is important to collect this solution in a solvent, e.g. ethanol, to slow down the condensation of tungstic acid [66]. The solution is always maintained under continuous magnetic stirring. After partial evaporation of the solvent with a rotavapor, an organic stabilizer is added to the tungstic acid. The stabilizer used was poly(ethylene glycol)-200 (PEG-200), and WO_3/PEG-200 ratio was $\approx$ 0.5 w/w. The resulting viscous, yellow sol could be used within 72 h, whereupon a precipitate was formed. The synthetic route is schematically illustrated in figure 2.1.

2.1.2 Upconverting nanoparticles synthesis

The synthesis of the UCNPs has been conducted by Dr. Marta Quintanilla at INRS-EMT (group of Prof. F. Vetrone). The synthetic route to prepare upconverting nanoparticles allows to control the nanoparticle size, morphology, and crystalline phase [44]. A thermal decomposition synthesis that relies on the decomposition of fluoride precursors of lanthanide ions at high temperature was adopted. $NaGdF_4$:Er^{3+}, Yb^{3+} UCNPs were prepared via a thermal decomposition process already reported in the literature [67]. In the process, lanthanide trifluoroacetates, used as precursors, were prepared from lanthanide oxides (Alpha Aesar, Gd_2O_3, Er_2O_3, Yb_2O_3, >99.99%) dissolved in deionized water and trifluoroacetic acid (Al-

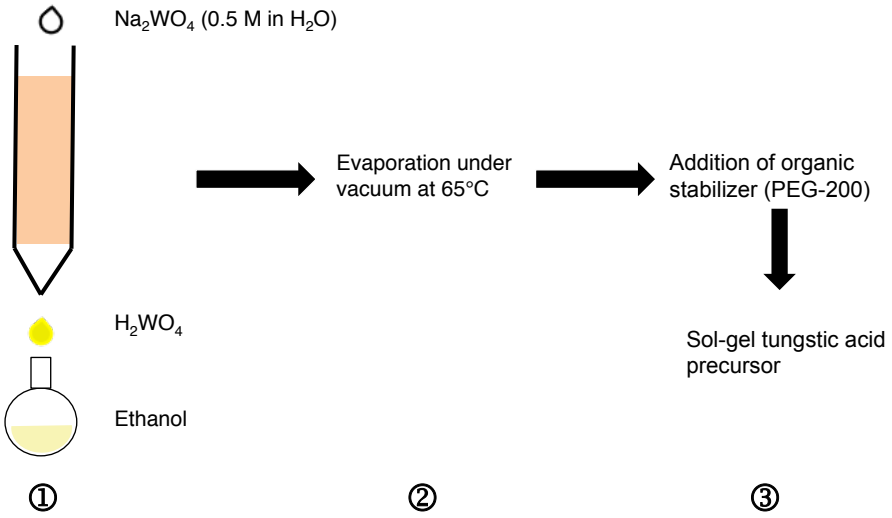

Figure 2.1 Process flow of the synthesis of WO_3. In the first step, an aqueous solution of Na_2WO_4 is passed through a proton-exchange resin. Then, H_2WO_4 is collected in ethanol. After the evaporation of the solvent, an organic stabilizer (PEG-200) is added. As prepared sols could be used within 72 h.

pha Aesar, 99%). The obtained precursors, together with the required stoichiometric amount of sodium trifluoroacetate (Sigma-Aldrich, 98%), were injected at a rate of 1.0 mL/min in a 1:1 solution of oleic acid (Alpha Aesar, 90%) and octadecene (Alpha Aesar, 90%) at 315°C and aged for 1 h. Oleic acid acts as the coordinating ligand, and octadecene as the reaction solvent. The role of the reaction solvent is to have a high boiling point solution, so as the decomposition of the fluoride precursors of lanthanide can occur.

The as prepared $NaGdF_4$:Er^{3+}, Yb^{3+} UCNPs were then washed by centrifugation and re-dispersed in hexane. As synthesized, UCNPs are capped with oleic acid, i.e. they are hydrophobic. Oleic acid was removed thus rendering the UCNPs hydrophilic by a process reported in the literature [68]. The final UCNPs were normally $\approx$ 45 nm in diameter.

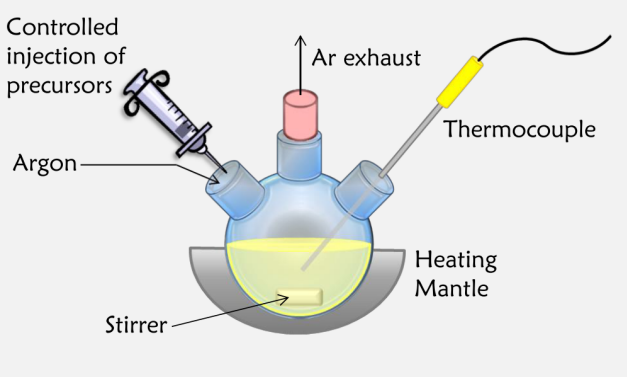

Figure 2.2 Illustration of the synthesis of UCNPs. After the preparation of the precursors, lanthanides trifluoroacetates are injected in oleic acid and octadecene at 315°C, before aging for 1 h at constant temperature. Image produced by Dr. Marta Quintanilla. Printed with permission from the creator.

2.1.3 Fabrication of the thin films

First, a mixture made from 1% weight/weight concentration of UCNPs suspension in water and ca. 0.3 M WO_3 solution was prepared and aged for at least 1h under continuous stirring. Several UCNPs/WO_3 mol % ratios from 2 to 16 mol % UCNP/WO_3 were investigated. Thin films were obtained from drop-casting 10 μL of WO_3 or UCNP/WO_3 solution on ITO-patterned substrates, followed by a thermal treatment at 385 °C under the presence of O_2 (160 standard cubic centimeters per minutes) for 30 min.

2.2 Microfabrication of the electrodes

We fabricated planar devices in order to investigate the electrical properties of our thin films. Electrodes were patterned fromITO-coated glass ($L = 100$ μm, and width $W = 6000$ μm). The fabrication steps are detailed in sections 2.2.1 and 2.2.2.

2.2.1 General remarks

Microfabrication processes are commonly used to produce devices with micrometric dimensions, e.g. in microelectronics, and can usually be separated into three steps: photolithography, etching, and deposition. Microfabrication can be done on a wide variety of substrates, such as silicon wafers and glass. Photolithography is required to define patterns on the substrate. Basically, a photoresist, i.e. a polymer mixed with a photoactive component, is spin-coated on a substrate. Afterwards, the substrate is exposed through a photomask to UV light. When the patterns contained on the mask are exposed to a UV lamp, the exposed

portion of the photoresist covering the substrate becomes soluble or insoluble in a developer: in the former case, the photoresist is said to be 'positive', while it is said to be 'negative' in the latter case. After the development of the photoresist in a developer, patterns are transferred on the photoresist. Etching is used to selectively remove a portion of the film from the substrate. It can be achieved using several methods, such as plasma and wet eching. Then, deposition techniques can be used to add a layer on the device.

2.2.2 Microfabrication process

In the case of the work done during this master's thesis, the microfabrication process consists in two steps only: photolithography and etching. We used microfabrication to pattern ITO-covered glass (30 mm x 30 mm, <15 Ω/square, purchased from Colorado Concept Coating). An AFM image of a typical ITO substrate is shown on figure 2.3. Prior to the microfabrication step (process flow is indicated on figure 2.5), the substrate were sequentially cleaned in an ultrasonic bath of isopropyl alcohol (IPA) for 15 min, acetone for 15 min, IPA for 15 min, and dried with a N_2 flux. Then, the substrates were exposed to a UV-ozone treatment for 15 min, in order to remove the organic contaminants from the surface. Substrates were immediately taken to the clean room to proceed to the microfabrication step.

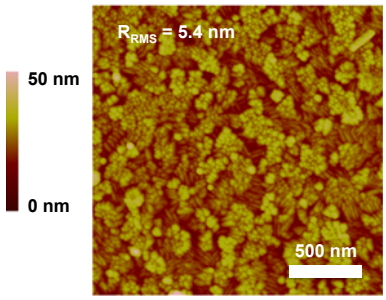

Figure 2.3 AFM topographical image of ITO substrate, as purchased from Colorado Concept Coating. Root mean square roughness (R_{RMS}) is about 5.4 nm (area is 2 × 2 μm).

Prior to the photolithography step, the substrates were placed into a Yield Engineering Systems Oven for 15 minutes for a dehydratation process under vacuum. When the substrate was cooled at room temperature, a positive photoresist (SPR 220 3.0) was spin-coated at 3000 rpm for 40 s to achieve a photoresist final thickness of about 3 μm. Then, the substrate was cured with a softbake at 115°C for 90 s. When the substrate was back at room temperature, the photoresist was exposed through a mask to a UV lamp using a Karl Suss MA4 mask aligner. The exposition time was adjusted to provide the optimal UV light dose to the photoresist. The optimal dose was found to be around 23 mJ/cm^2. Then, the substrate

underwent a post-exposure bake at 115°C for 90 s. The substrate was cooled down to room temperature, and after 5 minutes, the photoresist was developed for 3 min 40 s at room temperature using MF319 under continuous stirring.

Figure 2.4 Optical microscope image of the patterned electrodes prior to the chemical wet etching step.

Afterwards, chemical wet etching was used to remove the exposed ITO. The substrate was immersed in a hydrochloric acid (HCl) solution (HCl:H_2O 65 v/v%) for about 9 minutes, resulting in ITO-patterned electrodes with an interelectrode distance $L = 100$ μm, and width $W = 6000$ μm. Prior to the drop-casting of the solution (WO_3 or UCNP/WO_3), ITO-patterned substrates were cleaned again following the sequential procedure that was previously stated. The result of the microfabrication steps is ITO electrodes patterned on top of a glass substrate.

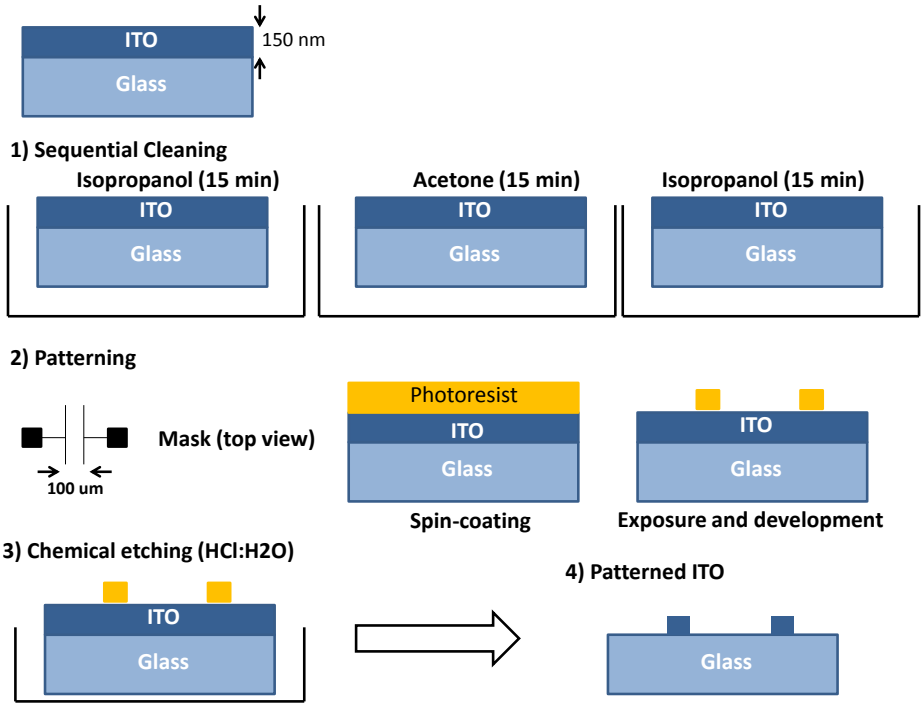

Figure 2.5 Microfabrication steps for planar ITO-patterned electrodes.

2.3 Characterization

In this section, the characterization techniques that were used during this master's project are presented: photoluminescence, X-ray diffraction, atomic force microscopy, and current-time measurements. The working principles will also be described.

2.3.1 Photoluminescence properties of UCNPs

Photoluminescence is the property some material has to emit light after the absorption of photons. In our case, we were intrerested in obtaining the photoluminescence spectrum of UCNPs. To do so, we excited the UCNPs with the proper wavelength to detect the light emitted by UCNPs after the upconversion process. Fluorescence hyperspectral imaging was used. The microscope can be used with a lamp source whose emission spectrum is close to a mercury lamp spectrum. During our experiments, light source was a portable continuous wave (cw) NIR laser emitting at 980 nm.

Photoluminescence measurements were achieved with Prism And Reflector Imaging Spectroscopy System (PARISS, purchased from LightForm Inc.) in ambient air condition and temperature under a 980 nm cw laser excitation. The PARISS system was used concomi-

tantly with a microscope (Olympus BX-51) spectrometer, a CCD camera, and a software (PARISS 8.0) to record the photoluminescence spectrum.

2.3.2 X-ray diffraction

X-ray diffraction permits to characterize the crystalline phases of a sample. First, an X-ray beam irradiates a sample, and is diffracted by the crystallographic planes of the sample. Then, the difference in the optical path caused by the reflection on the plane allows the beam to interfere with the beam reflected by other planes. It leads to the observation of constructive interference peaks, following the Bragg equation:

$$n\lambda = 2d\sin\theta$$

In our experiments, the crystalline structure of the UCNPs, WO_3, and UCNPs/WO_3 samples were performed in a Bruker D-8 Advance Diffractometer using CuKα radiation.

2.3.3 Atomic force microscopy

Atomic force microscopy (AFM) is a widely used characterization technique which permits obtaining topographical information of a sample. Working principle, as illustrated on figure 2.6, relies on the measurement of the deflection of the cantilever. Atomic force microscope is made of a feedback loop and a cantilever with a nanometric size silicon tip (tip radius $\approx$ 10 nm) at the end. AFM can be operated into two modes (figure 2.7). The first one is called 'contact mode', meaning that the tip is in contact with the sample. A constant force, corresponding to the deflection setpoint, is applied, such as the only allowed deflection is attributable to a change in the topography of the surface. This mode cannot be used with soft or fragile materials and is known to easily damage the tip. The second mode is the 'tapping mode'. It allows to circumvent the listed disadvantages of the contact mode. In this case, a force is applied to the end of the cantilever, such that the tip oscillates near the surface of the sample. When the tip is close to the surface, the amplitude of the oscillation reduces, and the tip is in contact with the sample for a short amount of time. The deflection of the cantilever is measured with a laser beam in the visible that is reflected by the tip to a photodetector. An acquisition software is used to record three dimensional images of a sample surface. The size of these images is variable and generally ranges between 1 and 100 μm. Once the topographical image is recorded, it is possible to obtain information on the surface under investigation, such as the profile, the roughness, the depth of holes, and size of the particles. A second image, called 'phase image' is also collected: it is the result of

a change in oscillation frequency of the cantilever during the scanning of the sample. This image can provide information on the physical and chemical properties of a sample. For example, it is possible to distinguish between two different materials on a phase image, but it is not possible to identify what exactly are the materials. One can only say that the two materials are different.

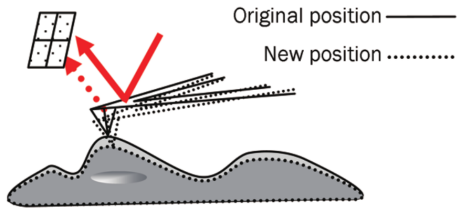

Figure 2.6 AFM working principle. A sample is placed under a silicon tip attached to a cantilever. Depending on the operating mode, the tip can be in contact or touch the sample intermittently. The deflection of the cantilever allows to obtain information on the topography of the sample investigated. Reproduced from [5].

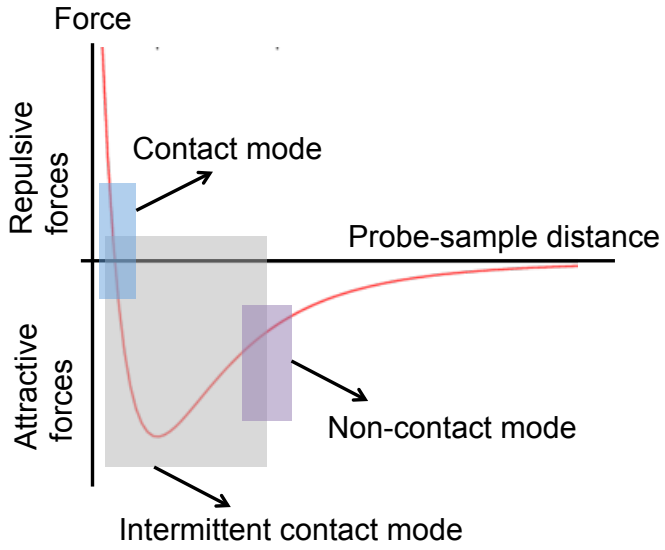

Figure 2.7 Comparison of the two operating modes. In contact mode, the sample and the tip are in contact, and the deflection of the cantilever is proportionnal to the forces acting on the tip. In tapping mode, the tip oscillates near the surface at a given frequency, resulting in a change of the amplitude of oscillation and force between the tip and the sample.

.

Every AFM image produced in this work was obtained in ambient air condition using a Veeco Dimension 3100 Digital Instruments with Si cantilever (tip radius < 10 nm, spring constant 40 N/m) at a scan rate of 1 Hz in tapping mode.

2.3.4 Electrical measurements in dark and light conditions

Electrical measurements were used to investigate the possibility to generate a photocurrent in UCNP/WO_3 thin films. The experimental setup, consisting in a substrate holder, micromanipulators to contact the samples, a system-measure unit (SMU), and a computer is illustrated in figure 2.8. It was used to measure the current over time in our thin films under the application of constant bias.

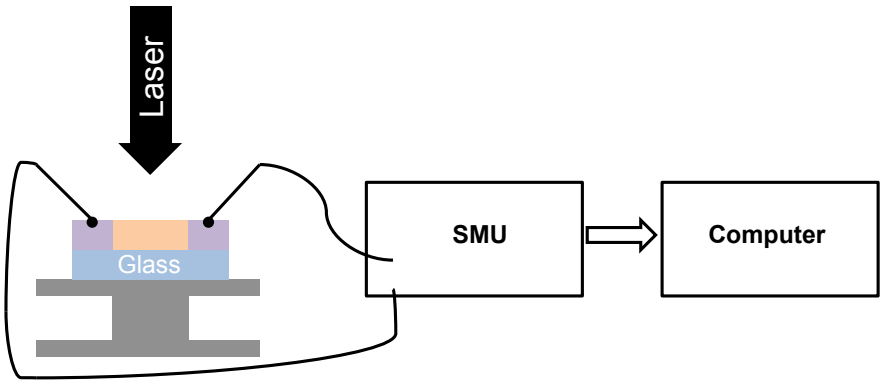

Figure 2.8 Setup for the electrical measurements. WO_3 or UCNP/WO_3 thin films were deposited on patterned substrates. A constant bias was applied, and the current was measured over time.

In our experiments, current-time measurements of WO_3 and UCNP/WO_3 films were carried out in planar configuration, in ambient air conditions, using a B2902A Agilent (SMU).

CHAPTER 3 ARTICLE 1: TOWARDS NEAR-INFRARED PHOTOSENSITIZATION OF TUNGSTEN TRIOXIDE NANOSTRUCTURED FILMS BY UPCONVERTING NANOPARTICLES

This chapter is the reproduction of an article submitted to the journal *RSC Advances* in June 2015. In this work, we make use of $NaGdF_4$: Er^{3+}, Yb^{3+} UCNPs to extend the absorption properties of solution-processed WO_3 to the NIR portion of the solar spectrum.

3.1 Authors

Frédéric Venne[a], Marta Quintanilla[b], Dilek Işik[a], Fiorenzo Vetrone[b,c], and Clara Santato[a,d]

[a.] Department of Engineering Physics, Polytechnique Montréal C.P. 6079 Succ. Centre Ville, Québec H3C 3A7, Canada

[b.] Institut National de la Recherche Scientifique - Énergie, Matériaux et Télécommunications (INRS - EMT), Université du Québec, 1650 Boul. Lionel-Boulet, Varennes, QC J3X 1S2, Canada

[c.] Centre for Self-Assembled Chemical Structures, McGill University, Montreal, Canada.

[d.] Regroupement Québécois sur les Matériaux de Pointe (RQMP).

3.2 Abstract

Upconverting materials are currently being explored in the field of solar energy conversion to extend to the near-infrared (NIR) the light harvesting properties of metal oxides, whose absorption is generally limited to the visible region of the solar spectrum. Here we propose to photosensitize nanostructured films of tungsten oxide (WO_3), a semiconductor widely investigated in photoelectrochemistry, photocatalysis and electrochromics, with $NaGdF_4$:Er^{3+}, Yb^{3+} upconverting nanoparticles (UCNPs). In order to do so, we fabricated nanocomposite films of WO_3 and NaGdF4:Er^{3+}, Y^{3+} UCNPs (indicated as UCNP/WO_3 films). Current-time measurements show that, under irradiation at λ = 980 nm, a relative increase in current of about 3% with respect to the dark current is observed in the UCNP/WO_3 films. The UCNP/WO_3 mol% ratio and the temperature of thermal treatment of the nanocomposite films are both critical to simultaneously achieve good photosensitization and charge carrier transport properties in the UCNP/WO_3 films.

3.3 Introduction

Photovoltaic (PV) solar energy conversion contributes to the fulfilment of the increasing world energy demand [69]. Different approaches have been investigated to overcome the Shockley-Queisser limit, which is the theoretical maximum efficiency attainable by a single-junction PV cell. As an example, multi-junction cells are intended to match the solar spectrum by stacking materials with increasing bandgaps [70]. Approaches based on optical processes, such as two-photon absorption (concurrent absorption of two photons by a material), downconversion (conversion of a high-energy photon to several low-energy photons) or upconversion (conversion of several low-energy photons into one high-energy photon) are also intensively pursued [71, 72, 48].

High surface area, mesoporous, transparent nanostructured films of metal oxides, such as TiO_2 and WO_3, have been widely investigated for solar energy conversion (photocatalysis and photoelectrochemistry) and energy conservation (electrochromism) [73, 38, 74, 75]. However, their large bandgaps (ca. 3.1 eV for TiO_2 and ca. 2.5 eV for WO_3) render imperative the search for strategies to improve their solar light absorption properties, from the viewpoint of practical PV applications. In particular, the photoresponse of WO_3 extends to 500 nm, such that photons of lower energy, e.g. NIR photons, are not harvested to generate photocurrent, thus leading to considerable energy losses [65, 2].

Given their optical properties, upconverting (UC) materials are presently investigated for biomedical [76, 77, 78], photocatalysis [79, 80, 81, 82] and solar energy conversion applications [50, 83, 84, 56]. Indeed, in UC materials the excitation of the higher energy emitting states occurs via the sequential excitation of multiple NIR photons. In particular, in lanthanide-based upconverting nanoparticles (UCNPs), upconversion occurs through *real*, long lifetime $4f$ excited states of the lanthanide species, in contrast to conventional two-photon excited materials. As a consequence, ultrafast femtosecond lasers are not required and upconversion can be induced by low power, continuous wave (cw) diode lasers. Fluoride-based crystals, in particular $NaGdF_4$, are commonly employed as host materials for lanthanide dopants, due to their low phonon energies, helping to limit non-radiative relaxation processes [85].

Combining UC materials and metal oxide semiconductors represents an interesting approach to photosensitize the semiconductors in the NIR region of the solar spectrum, since the photons absorbed by the UC material can, after upconversion, be harvested by the semiconductor to eventually generate a photocurrent [56, 86, 87, 88, 89, 57, 90].

UC materials are often included in a solar energy conversion system in the form of an external

layer, with different possible configurations, such as PV cell and rear converter or front converter and PV cell [91, 51]. On the other hand, the use of UCNPs in intimate contact with nanostructured semiconductors has the potential to create a maximized positive synergy between the two nanomaterials.

In this work, we report on the design, fabrication and characterization of nanocomposite films based on sol-gel prepared WO_3 and NaGdF4:Er^{3+}, Yb^{3+} UCNPs to improve the absorption properties of WO_3 nanostructured films in the NIR region of the solar spectrum. Our approach to use $NaGdF_4$:Er^{3+}, Yb^{3+} UCNPs to photosensitize WO_3 was based on the fact that, when excited at λ_{exc} = 980 nm, the UCNPs have two emission bands in the visible range, partly overlapping with the absorption spectrum of WO_3 [67, 41], thus leading to the possibility to use them as photosensitizers. The measure of the photocurrent generated by UCNP/WO_3 films in planar configuration under NIR irradiation (λ_{exc} = 980 nm) confirmed the interest of our approach. Atomic Force Microscopy (AFM), X-ray diffraction (XRD) and photoluminescence (PL) studies were conducted to identify the fabrication conditions to achieve simultaneously good photosensitization and charge carrier transport properties in the UCNP/WO_3 nanocomposite films.

3.4 Experimental section

3.4.1 Microfabrication of the electrodes

ITO electrodes were patterned by photolithography. ITO-coated glass substrates (Colorado Concept Coatings, 30 mm x 30 mm, $<$ 15 Ω/square sheet resistance) were sequentially cleaned in an ultrasonic bath in isopropyl alcohol (IPA), acetone, and IPA for 15 min each, and N_2-dried. Prior to the microfabrication steps, ITO substrates were exposed to a UV-ozone treatment for 15 min. After selective exposure and development of a positive-tone photoresist layer, the ITO film was chemically etched with hydrochloric acid (HCl:H_2O 65 v/v%) and the unexposed photoresist was removed with acetone. This process resulted in ITO electrodes with an interelectrode distance L of 100 μm and width W of 6000 μm.

3.4.2 Materials and fabrication of the thin films

WO_3 was prepared following a sol-gel synthesis already reported in the literature [65]. Na_2WO_4, PEG-200, ethanol and the proton-exchange resin (Dowex 50WX2) were purchased from Sigma Aldrich. $NaGdF_4$:Er^{3+}, Yb^{3+} (2 mol% Er^{3+}, 20 mol% Yb^{3+}) UCNPs were prepared via a thermal decomposition process already reported in the literature [67]. First, lanthanide trifluoroacetates used as precursors in the synthesis were prepared from lanthanide oxides (Alpha

Aesar, Gd_2O_3, Er_2O_3, Yb_2O_3, >99.99%) in deionized water and trifluoroacetic acid (Alpha Aesar, 99%) [92]. In a standard process, the obtained precursors, together with the required stoichiometric quantities of sodium trifluoroacetate (Sigma-Aldrich, 98%), were injected at a rate of 1.0 mL/min in a 1:1 solution of oleic acid (Alpha Aesar, 90%) and octadecene (Alpha Aesar, 90%) at 315°C, and aged for 1 h. The prepared β-phase $NaGdF_4$:Er^{3+}, Yb^{3+} UCNPs were then washed by centrifugation and redispersed in hexane. The synthesized UCNPs are capped with the long-chained oleate molecules making them hydrophobic. To render them hydrophilic and to avoid any possible effect of the capping agent in the final material, we removed the oleates by following a process described in literature [68]. The UCNPs had a narrow size distribution, with 45 nm in diameter (figure 3.1 (a)), and showed the hexagonal-nanoplate shape typical of the β-phase of $NaGdF_4$.

To fabricate the nanocomposite films, a mixture containing 1% weight/weight concentration of UCNPs suspension in water and ca. 0.3 M tungstic acid sol was prepared to reach a $\approx$ 8 mol% UCNP/WO_3. The mixture was aged for about 1 h under continuous stirring before film deposition. Nanocomposite films were obtained by drop-casting 10 μL UCNP/WO_3 mixture (or WO_3 sol for control films) on ITO-patterned substrates, followed by a thermal treatment at 385°C, in O_2 (160 scc min^{-1}), for 30 min.

3.4.3 Characterization

Photoluminescence measurements were carried out with a Prism And Reflector Imaging Spectroscopy System (PARISS, purchased from LightForm Inc.) in ambient air conditions after excitation at λ_{exc}=980 nm from cw NIR laser diode (power density = 1 W/cm^2). Transmission properties of WO_3 films were assessed using a PerkinElmer Lamba 1050 UV/Vis/NIR spectrophotometer. The structure of the samples was characterized by XRD (Bruker D-8 Advance Diffractometer), using CuKα radiation. High-resolution transmission electron microscopy (TEM, Philips CM200) was used to ascertain the phase, morphology, crystallinity and size distribution of the UCNPs. Atomic force microscopy (AFM) images were obtained in ambient air condition using a Veeco Dimension 3100 Digital Instruments with Si cantilever (tip radius <10 nm, spring constant 40 N/m) at a scan rate of 1 Hz. Photocurrent-time measurements were carried out in planar configuration (figure 3.1 (b)), in ambient air conditions, using a B2902A Agilent Source Measure Unit (SMU).

3.5 Results and discussion

3.5.1 Thin film preparation and characterization

To achieve the successful combination of UCNPs and nanostructured WO3 in a nanocomposite film, we had to overcome a number of challenges.

First, since UCNPs are electrically insulating, it was imperative that we identify the optimal UCNP/WO_3 mol% ratio to photosensitize WO_3 without hindering charge transport in the nanocomposite films. In order to do so, we prepared films from UCNP/WO_3 mol% ratios ranging between 1 and 16 mol%. Films prepared at ratios above 8 mol% were discontinuous, i.e. not easily amenable to incorporation into devices (figure 3.4). No significant effect of the presence of UCNPs was observed in films with ratios below 8 mol%. The morphology of these films was indeed similar to that of WO_3 control films (shown figure 3.1 (c)). 8 mol% UCNP/WO_3 films, similarly to the case of WO_3 control films, showed complete substrate surface coverage (figure 3.1 (d)). Furthermore, 8 mol% UCNP/WO3 films showed no evidence of phase segregation and values of the roughness (R_{RMS}) comparable to those of WO_3 films (0.8 vs 0.9 nm). Therefore, overall, 8 mol% UCNP/WO_3 films showed to be of device quality.

Secondly, we had to identify the optimal temperature for the thermal treatment of the nanocomposite films to ensure good charge transport in the films, while keeping good UCNPs emission, required for photosensitization. Achieving good transport properties in nanostructured WO_3 films synthesized by sol-gel methods usually require thermal treatment temperatures within the range 300 – 600 °C [93, 35]. However, such high temperatures could affect the crystalline structure of UCNPs. Indeed, a change from the hexagonal phase (β-UCNPs) to the cubic phase (α-UCNPs) was expected to take place at temperatures as low as 400 °C [61]. Importantly, the UC process is reported to be one order of magnitude more efficient in β-phase $NaGdF_4$:Er^{3+}, Yb^{3+} UCNPs than in α-UCNPs, for the nanoparticle size used here [46]. To try to avoid, at least in part, this phase change, we treated the UCNP/WO_3 films at 385 °C. The comparison of the PL spectrum of 45 nm-sized $NaGdF_4$:Er^{3+}, Yb^{3+} β-UCNPs treated at 385 °C with the optical transmission spectrum of 1 μm-thick WO3 films treated at 385 °C shows the overlap of the WO_3 absorption and the UCNPs emission (figure 3.1 (e)). Such an overlap constitutes the foundation of our photosensitization approach. Importantly, two emission bands located at ca. 550 nm and ca. 660 nm are observable upon NIR laser excitation (λ_{exc}=980 nm, power density=1 W/cm^2) in the PL spectra of the UCNPs, both after room temperature drying and 385 °C thermal treatment (figure 3.1 (e), inset). The green emission band located at ca. 550 nm is attributed to transitions from the $^2H_{11/2}$ and $^4S_{3/2}$ excited states to the $^4I_{15/2}$ ground state of Er^{3+} ions (figure 3.5). The red emission band

observed at ca. 660 nm is attributed to the transition from the $^4F_{9/2}$ excited state to the $^4I_{15/2}$ ground state [85]. Figure 3.1 (e) shows that the thermal treatment affects the emission properties of the UCNPs: the green:red intensity ratio is about 1 when the UCNPs are dried at room temperature, whereas this ratio falls down to 0.3 after treatment at 385 °C, likely due to a change in UCNPs structure with the thermal treatment.

XRD measurements were then performed to gain insight on the dependence of the PL properties on the temperature of thermal treatment (figure 3.2). When dried at room temperature (RT) on glass, the XRD peaks of $NaGdF_4$:Er^{3+}, Yb^{3+} UCNPs (pattern 1) match the filed pattern of NaGdF4 with hexagonal crystal phase (β-phase)[1] [6]. When the UCNPs are thermally treated at 385 °C (pattern 2), UCNPs are likely to remain in the β-phase, as suggested by the presence of the peaks at 30, 43, and 52°. The positions of the peaks of the cubic phase (α-UCNPs) are also indicated in figure 3.2, to validate the hypothesis that UCNPs are not in the α-phase after the thermal treatment. The comparison between pattern 1 and 2 show that the relative intensity of the peaks changes from pattern 1 to pattern 2 thus suggesting that the UCNPs reorient during thermal treatment. This reorientation can account for the some differences in the upconverted red and green emissions since $NaGdF_4$ is not isotropic [94]. The presence of O_2 during the thermal treatment has no noticeable effect on the structure of the UCNPs.

[1]The peak (0 0 2) was deduced using the Bragg diffraction law. It was not indexed from [6]

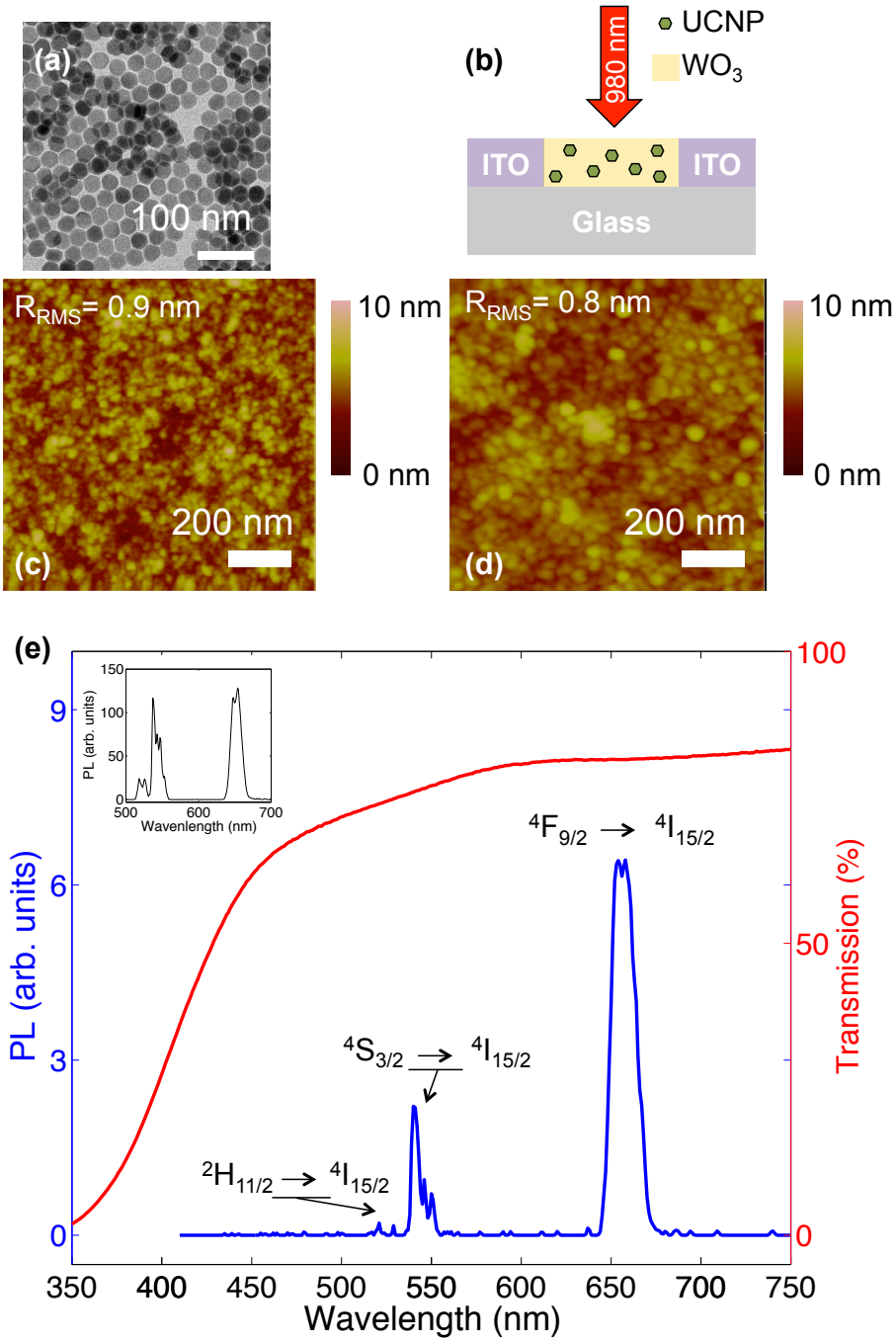

Figure 3.1 (a) TEM image of β-$NaGdF_4$:Er^{3+}, Yb^{3+} UCNPs. (b) Experimental configuration adopted for the electrical characterization (photocurrent vs time). Topographical AFM images of (c) WO_3 and (d) 8 mol% UCNP/WO_3 films, deposited on glass, treated at 385°C. (e) PL spectrum of β-$NaGdF_4$:Er^{3+}, Yb^{3+} UCNPs drop-cast on glass and thermally treated at 385°C (right y axis) and optical transmission spectrum of a WO_3 film ($\approx$1 μm in thickness), deposited on glass and thermally treated at 385°C (right y axis). Inset figure 3.1(e): PL spectrum of the UCNPs, drop-cast on glass and dried at room temperature.

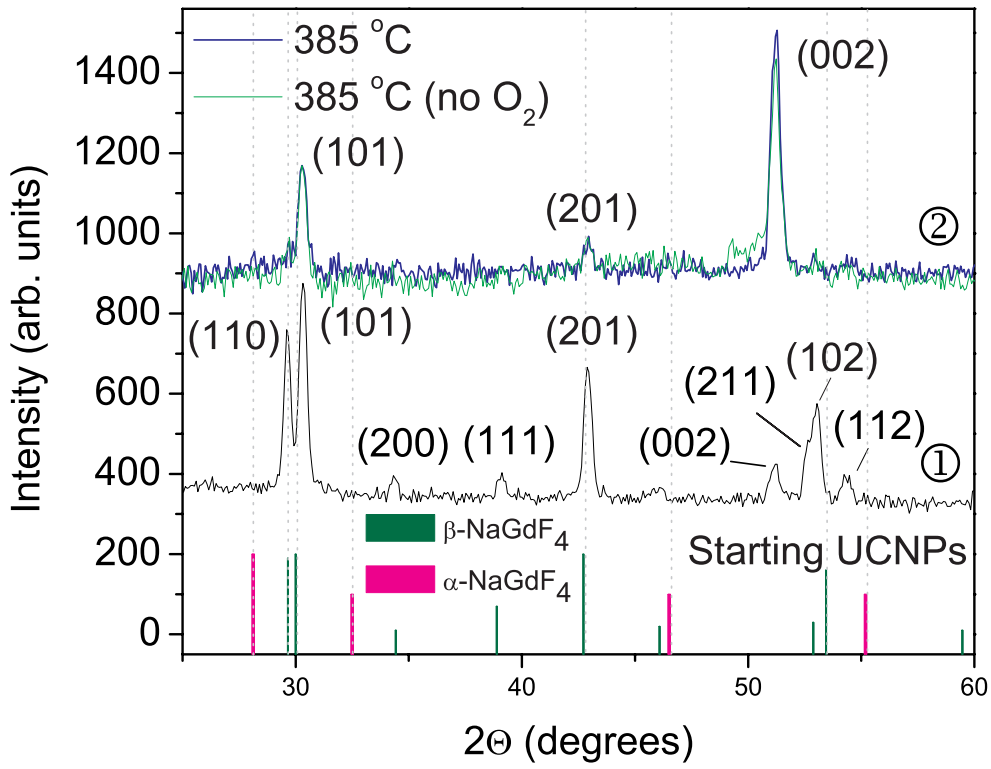

Figure 3.2 XRD patterns of β-UCNPs, 45 nm in diameter, drop-cast on glass. After room temperature drying and thermal treatment at 385°C, UCNPs are in the β-phase (hexagonal phase, patterns 1 and 2). The peak positions for the α and β phases are included at the bottom of the figure [6].

3.5.2 Electrical Measurements

Current-time measurements were performed using a two-electrode, planar configuration in order to assess the possibility to generate a photocurrent in UCNP/WO_3 nanocomposite films exposed to NIR light (XRD pattern in figure 3.6). To this purpose, UCNP/WO_3 nanocomposite films were systematically compared with WO_3 control film samples. During the electrical measurements, the films were initially kept in ambient light conditions for 300 s, followed by 300 s in dark, under constant electrical bias (0.5, 0.7, or 1.0 V), to permit the dark current to stabilize prior to photocurrent measurements. Afterwards, the samples were illuminated by a cw NIR laser (λ_{exc}=980 nm, power density=1 W/cm^2). Typically, during the electrical measurements the films were exposed for 30 s to light, followed by 60 s in the dark. We used the "on/off ratio", R, computed as follows:

$$R = 100 \times \frac{i_{on} - i_{off}}{i_{off}} \tag{3.1}$$

where i_{on} the current when the NIR laser is shed on the sample (on current), and i_{off} the current when the NIR laser is switched off (off current) to describe the effect of the illumination on the current measured. When 8 mol% UCNP/WO_3 films are exposed to NIR light, an increase of the current was observed (figure 3.3(a)). A value of R ranging between 3.4 to 3.9% was obtained when the NIR light was shed on the nanocomposite films, depending of the applied electrical bias. This increase in the current is attributable to the absorption of the NIR light by the UCNPs followed by the harvesting of the upconverted light by the WO_3, in turn followed by the generation of a photocurrent.

To evaluate the possibility that thermal effects due to the laser exposure are responsible for the current increase observed with 8 mol% UCNP/WO_3 films exposed to NIR light, we exposed WO_3 control films to the NIR laser: no noticeable current increase was observed in this case (figure 3.3(b)). These results suggest that the increase in the current measured from 8 mol% UCNP/WO_3 nanocomposite films under NIR exposure might be a photocurrent induced by the presence of UCNPs, and that thermal effects likely play a minor role.

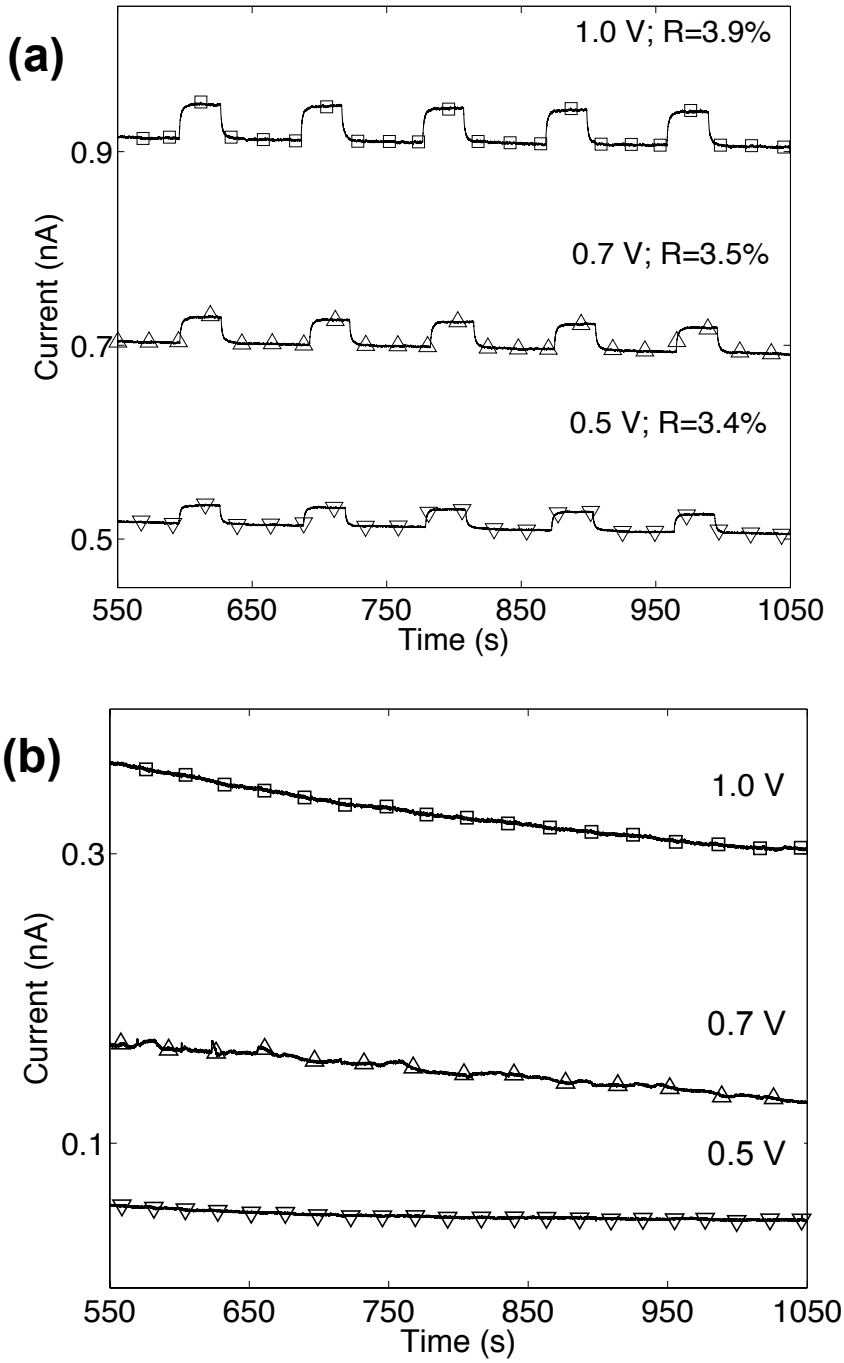

Figure 3.3 Current-time measurements under NIR chopped light (60 s in the dark and 30 s under irradiation, λ_{exc}=980 nm, power density=1 W/cm^2) for films deposited on patterned ITO with an interelectrode distance of 100 μm and thermally treated at 385°C made of (a) 8 mol% UCNP/WO_3 and (b) WO_3 (see figure 3.7). Samples were kept under constant electrical bias for 300 s in ambient light conditions, followed by 300 s in the dark, before chopping the light.

3.6 Conclusions and perspectives

In conclusion, we observed an increase in the current measured in $NaGdF_4$:Er^{3+}, Yb^{3+}/WO_3 nanocomposite films under NIR (λ_{exc}=980 nm) irradiation, with respect to dark conditions. After a judicious choice of the mol% ratio in the nanocomposite film and the temperature of the thermal treatment we demonstrate that nanocomposite films can be engineered so as not to hinder the transport properties in the nanocomposite films when extending the photosensitivity of the WO_3 to the NIR light. The approach herein presented is interesting for solar energy conversion applications, as it permits to prepare, by an easy solution-based technique, high surface area, nanocomposite films photosensitive to visible and NIR light. We are now working towards the assessment of the universality of our nanocomposite approach. We recently obtained interesting preliminary results using blue-emitting UCNPs, such as $LiYF_4$: Tm^{3+}, Yb^{3+}, that improve the overlap between the absorption spectrum of WO3 and the emission spectrum of UCNPs.

In perspective, several challenges have to be addressed to optimize the use of UCNPs as metal oxide photosensitizers. Considering that the absorption bandwidth of the lanthanide-based UCNPs is narrow (usually limited to a few nanometres), the combination of several upconverters within the metal oxide matrix should be explored.

3.7 Acknowledgements

The authors are grateful to J. Lerner (LightForm Inc) and P. Moraille for fruitful discussions and to Y. Drolet for technical support. This work was financially supported by: NSERC (Discovery grants C.S. and F.V.), FRQNT Team Grant (C.S. and F.V.), MDEIE (F.V.). F. Venne acknowledges the financial support provided by CMC Microsystems (MNT program) and M. Quintanilla acknowledges the financial support of Fundacion Ramon Areces.

3.8 Supplementary information to article 1: Towards Near-Infrared Photosensitization of Tungsten Trioxide Nanostructured Films by Upconverting Nanoparticles

This section is the reproduction of the supplemementary information to the article submitted to the journal *RSC Advances* in June 2015. In this work, we make use of $NaGdF_4$: Er^{3+}, Yb^{3+} UCNPs to extend the absorption properties of solution-processed WO_3 to the NIR portion of the solar spectrum.

3.8.1 Authors

Frédéric Venne[a], Marta Quintanilla[b], Dilek Işik[a], Fiorenzo Vetrone[b,c], and Clara Santato[a,d]

[a.] Department of Engineering Physics, Polytechnique Montréal C.P. 6079 Succ. Centre Ville, Québec H3C 3A7, Canada

[b.] Institut National de la Recherche Scientifique - Énergie, Matériaux et Télécommunications (INRS - EMT), Université du Québec, 1650 Boul. Lionel-Boulet, Varennes, QC J3X 1S2, Canada

[c.] Centre for Self-Assembled Chemical Structures, McGill University, Montreal, Canada.

[d.] Regroupement Québécois sur les Matériaux de Pointe (RQMP).

3.8.2 Supplementary information

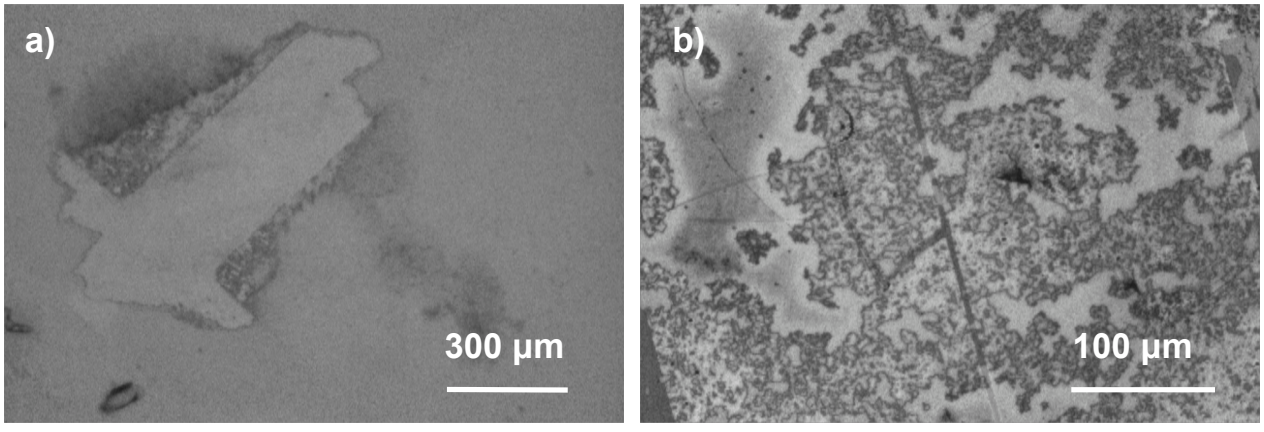

Figure 3.4 Optical microscope images of 16 mol% UCNP/WO_3 films thermally treated at 385°C deposited on a) glass substrate and b) SiO_2.

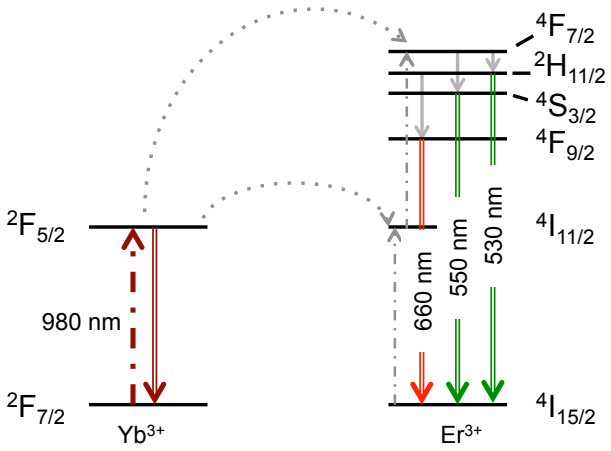

Figure 3.5 Partial $NaGdF_4$:Er^{3+}, Yb^{3+} UCNPs energy levels diagram.For the sake of clarity, only the energy levels involved in the upconversion process are shown. Dashed lines are associated to energy absorption, dotted lines are associated to energy transfer, full grey lines are associated to non-radiative processes, and full double lines are associated to radiative processes.

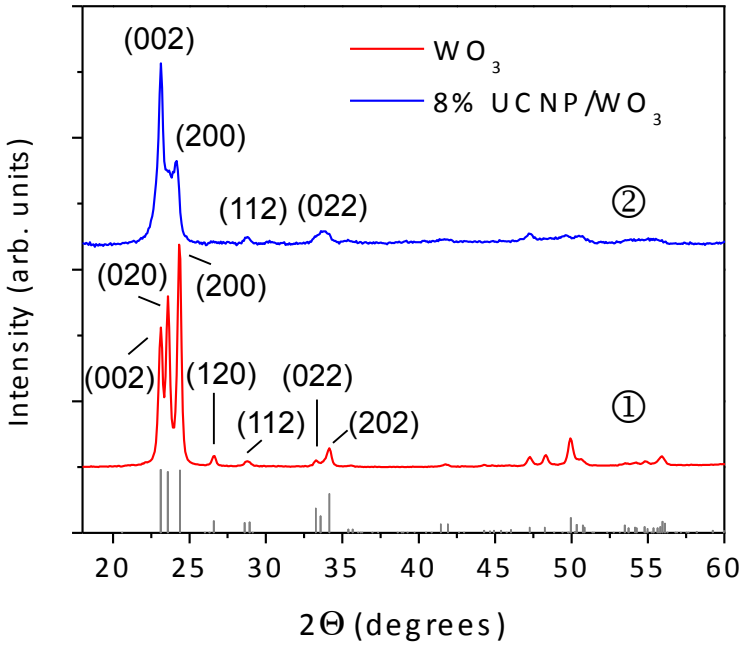

Figure 3.6 XRD measurements of WO_3 (pattern 1) and 8 mol % UCNP/WO_3 thin films deposited on glass substrate and thermally treated at 385°C (pattern 2).

Comments on figure 3.6: XRD measurements were performed to assess the structure of WO_3 and 8 mol% UCNP/WO_3 thin films. The XRD pattern of WO_3 thin films shows three sharp peaks in the 22-25° region, two peaks in the 26-29° region, and two peaks in the 32-35° region (figure 3.6, pattern 1): the peaks are indexed to the planes of monoclinic WO_3 (ICDD # 00-043-1035). 8 mol% UCNP/WO_3 thin films annealed at 385°C show two peaks in the 22-25° region, one centered at 28.8° and another centered at 33.7° (figure 3.6, pattern 2). No peaks from UCNPs were observed in the pattern from UCNP/WO_3 thin films, probably because of the excessively low concentration of UCNPs. A slight shift in the position as well as a broadening of the peaks is observed when WO_3 films contain UCNPs.

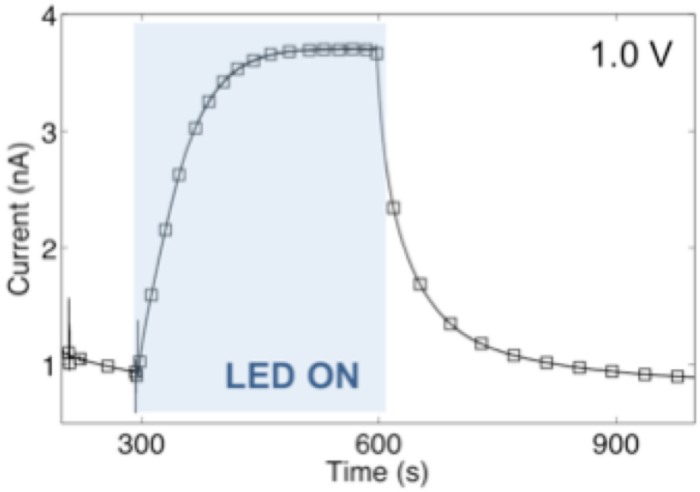

Figure 3.7 Current-time measurements of pure WO_3 thin films thermally treated at 385°C deposited on patterned ITO with an interelectrode distance of 100 μm under LED white light (Thorlabs, model LIU004). Initially the sample was kept in dark conditions for 300 s at an applied electrical bias of 1 V, followed by 300 s under LED white light, followed by dark conditions.

CHAPTER 4 COMPLEMENTARY RESULTS

In this chapter, we present results not included in article 1 that complement the work done during this master's thesis.

4.1 Choice of the configuration

In this section, the results collected in the first months of the project are presented. These results justify the approach adopted for article 1. First, we present the results that prompted the choice of the experimental configuration used in the article.

We evaluated the possibility to use the UCNPs in "layered" and "nanocomposite" configuration, as shown on figure 4.1. In the former case, the UCNPs are deposited on top of a WO_3 thin film, while the UCNPs are embedded in the WO_3 thin film in the latter case (nanocomposite configuration).

Figure 4.1 Two configurations investigated at the beginning of the project. a) "Layered" configuration: the UCNPs are deposited on a WO_3 thin film. b) "Nanocomposite" configuration: the UCNPs are embedded in the WO_3.

We investigated the PL properties of samples prepared in layered configuration (figure 4.2). Hexagonal or cubic UCNPs were drop-cast on WO_3 and dried at room temperature. Samples were then irradiated with a 980 nm cw NIR laser and PL spectrum was recorded. We concluded from this experiment that the layered configuration cannot be used, because WO_3 samples with UCNPs on top have the same PL properties than the pure UCNPs films (independently from the phase of the UCNPs). It means that there is no significant interaction between the two materials, i.e. that upconverted light is not significantly harvested by WO_3. This experiment prompted our choice to adopt the nanocomposite configuration.

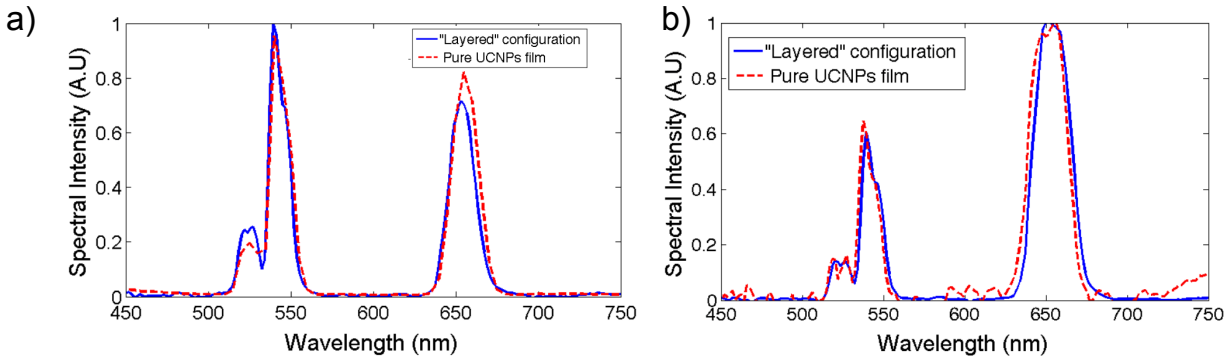

Figure 4.2 PL properties of a) hexagonal b) cubic phase UCNPs deposited on WO_3 (full lines). The PL properties of a thin film made from pure UCNPs (dashed lines), drop-cast on a glass substrate are also shown for reference.

4.2 Effect of the thermal treatment temperature on UCNPs photoluminescence properties

We also studied the effect of the thermal treatment on hexagonal UCNPs PL properties by drop-casting UCNPs on a glass substrate and treating them at different temperatures (room temperature, 400°C, and 550°C). The results are shown on figure 4.3. We see that the temperature strongly affects the green emission of the UCNPs. At 550°C (the temperature usually required to treat sol-gel prepared WO_3 thin films), the green emission almost totally vanishes. At 400°C, we see that the green emission is weak with respect to the red emission. The main conclusion from this experiment is that we have to carefully choose the temperature of the thermal treatment to maintain the PL properties of the UCNPs.

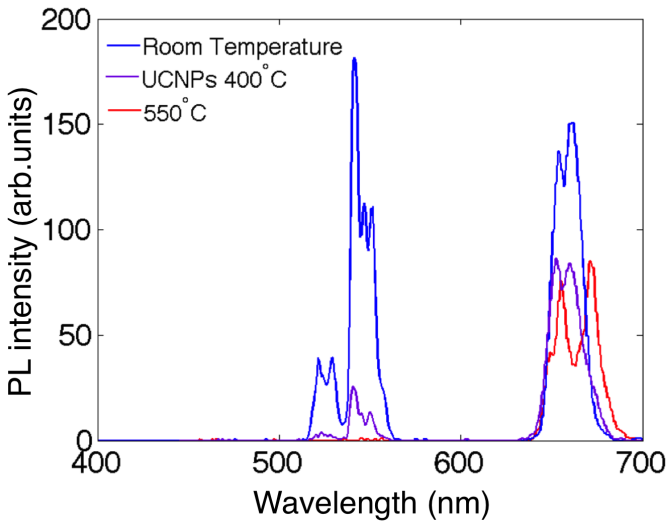

Figure 4.3 PL intensity of pure hexagonal UCNPs treated at different temperatures. Size of the UCNPs is 35 nm. UCNPs dispersed in water were drop-cast on a glass substrate and thermally treated at RT, 400°C, and 550°C. Green emission is strongly affected by the temperature of the thermal treatment.

4.3 Effect of the UCNPs size

To shed light on the effect of the UCNPs size on the photocurrent process, we prepared two kinds of samples: one containing 35 nm-sized hexagonal UCNPs and one containing 95 nm-sized hexagonal UCNPs. As shown on figure 4.4, we observed an increase in current (of about 1.5% with respect to the dark current) when a 980 nm laser was shed on samples containing 35 nm-sized hexagonal UCNPs, whereas no noticeable current increase was observed in samples containing 95 nm-sized hexagonal UCNPs. The major conclusion that we drew from this experiment is that it seems preferable to use 'small' UCNPs, rather than larger ones. In the former case, the size of the UCNPs is comparable to the size of WO_3.

The increase in current with respect to the dark current for 8 mol %UCNPs/WO_3 thin films made from 35 nm UCNPs is lower than what we reported for 8 mol %UCNPs/WO_3 thin films made from 45 nm UCNPs. This result could stem from two factors. First, the temperature of the thermal treatment for the results presented on figure 4.4 was higher (400°C) than the temperature that was used for the experiments presented in the article (385°C). As discussed in the article, the emission properties of the UCNPs are strongly affected by the temperature of the thermal treatment. Secondly, the UCNPs used for the article were about 45 nm in diameter. Smaller UCNPs are more sensitive to surface defects than larger UCNPs, which might result in less efficient upconversion process.

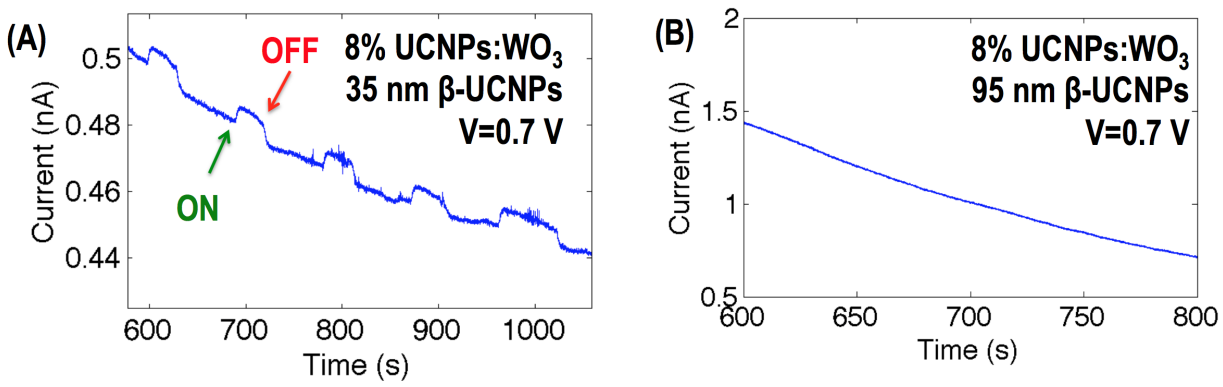

Figure 4.4 Current-time measurements of thin film samples deposited on substrates patterned with ITO electrodes and thermally treated at 400°C. The samples were kept under electrical bias (V=0.7 V) for 5 min in ambient light conditions followed by 5 minutes in the dark before chopping the light (λ_{exc}=980 nm). Nanocomposite films containing 8 mol %UCNPs/WO_3 with (A) 35 nm-sized hexagonal UCNPs and (B) 95 nm-sized hexagonal UCNPs.

The main conclusions from these early experiments are:

1. A nanocomposite configuration appears more promising than a layered configuration;

2. The temperature of the thermal treatment strongly affects the PL properties of the UCNPs. For this reason, we decided to treat the samples at 385°C in order to preserve the UCNPs green emission;

3. It appears more promising to use 45 nm UCNPs, i.e. UCNPs whose size is approximately the same as WO_3 particles, rather than large UCNPs (e.g. 95 nm) or small UCNPs (e.g. 35 nm).

4.4 Towards a better understanding of the results presented in article 1

In this section, we present complementary experiments that were carried out to gain a better understanding of the results included in the article. We present and discuss current-time measurements performed under different irradiation conditions (white LED and chopped NIR laser) and temperature-dependent current-time measurements of 8 mol % UCNP/WO_3 thin films.

4.4.1 Current-time measurements of 8 mol % UCNP/WO_3 thin films under white light

8 mol % UCNP/WO_3 thin films deposited on ITO-patterned substrates and thermally treated at 385 °C were exposed to a white LED light (Thorlabs, model LIU004). As shown on figure 4.5, an increase in current is observed when the LED is shed on the sample. The photoresponse of the UCNP/WO_3 thin film is slow and the current does not saturate after more than five minutes. When the sample is back in dark conditions, the current slowly decreases. The slow increase is tentatively attributed to the trapping of charge carriers at the surface of UCNPs. The slow decrease of the current in dark conditions could also originate from the trapping of charge carriers.

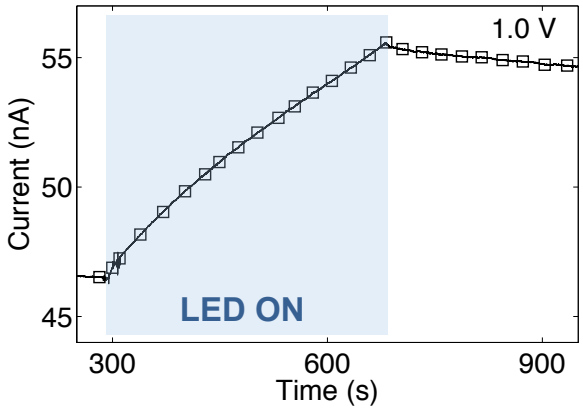

Figure 4.5 Current-time measurements of UCNP/WO_3 (8 mol %) thin films thermally treated at 385 °C deposited on patterned ITO with an interelectrode distance of 100 μm under white LED light (Thorlabs, model LIU004). Samples were kept under constant electrical bias (1 V) for 300 s in dark conditions, followed by 300 s under white LED light, followed by dark conditions. An increase in current is observed when the white LED is shed on the sample.

4.4.2 Current-time measurements of 8 mol % UCNP/WO_3 thin films under chopped light at variable frequency

We achieved current-time measurements in 8 mol % UCNP/WO_3 thin films under chopped NIR laser (λ_{exc}=980 nm, power density $\approx$ 5 W/cm^2) at variable chopping frequency. The main motivation was to try to validate the hypothesis that the increase in current in 8 mol % UCNP/WO_3 thin films under λ_{exc}=980 nm was due to optical processes rather than thermal processes. Optical processes in principle are faster than thermal ones. Samples were kept under constant electrical bias for 300 s in ambient light conditions, followed by 300 s in the dark. NIR laser was then chopped on the sample (at 1 or 0.5 Hz). For the two frequencies tested, the increase in current with respect to the dark current occurs in a time range shorter than 1 s. In order to rule out the hypothesis that thermal processes are contributing to the increase of the current upon 980 nm irradiation, the same experiments would have to be carried out at higher frequencies.

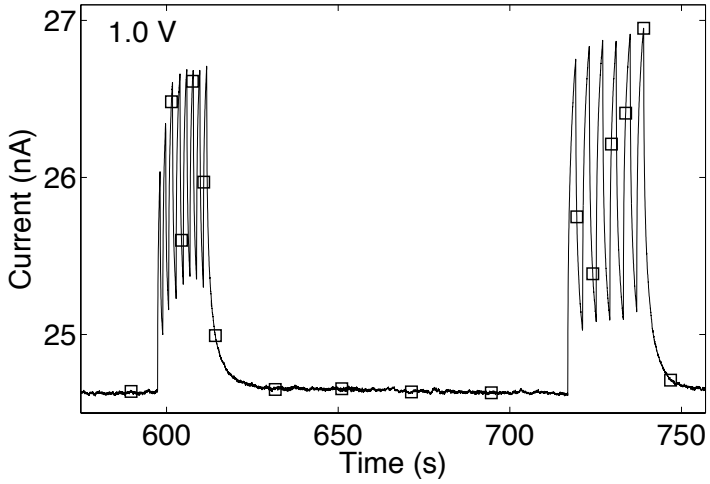

Figure 4.6 Current-time measurements under NIR chopped light for $\approx$ 8 mol % UCNP/WO_3. Thin films were deposited on patterned ITO with an interelectrode distance of 100 μm and thermally treated at 385°C. Samples were kept under constant electrical bias for 300 s in ambient light conditions, followed by 300 s in the dark. Frequency of chopping light was 1 Hz and 0.5 Hz, respectively.

4.4.3 Temperature-dependent current-time measurements of 8 mol % UCNP/WO_3 thin films under chopped light

We investigated the effect of the temperature of the substrate during current-time measurements for four temperatures (T_1=50°C, T_2=45°C, T_3=40°C and T_4= 35°C), as shown on figure 4.7. The motivation behind this experiment was to investigate to which extent the increase of the current under 980 nm irradiation was affected by the temperature of the sample, which could potentially help us in disentangling optical and thermal effects. The on/off ratio R, i.e. the relative increase in current with respect to the dark current, was computed as follows:

$$R = 100 \times \frac{i_{\text{on}} - i_{\text{off}}}{i_{\text{off}}} \tag{4.1}$$

The mean value of R was affected by the temperature of the substrate. The highest mean R is reported for the highest temperature used. The temperature affect the PL properties of UCNPs. Higher temperatures result in less efficient emission, which can be explained by the increase of the rate of non-radiative processes [95]. In this scenario, the increase in current reported on figure 4.7 is a competition between the better electrical conductivity of WO_3 and less efficient upconversion emission properties of UCNPs as a function of temperature. This result suggests that the improvment in the value of R might be associated to electron detrapping. To improve our current understanding of optical and thermal effects in our UCNP/WO_3 system, we have to measure the influence of the temperature on the photoluminescence properties of the UCNPs.

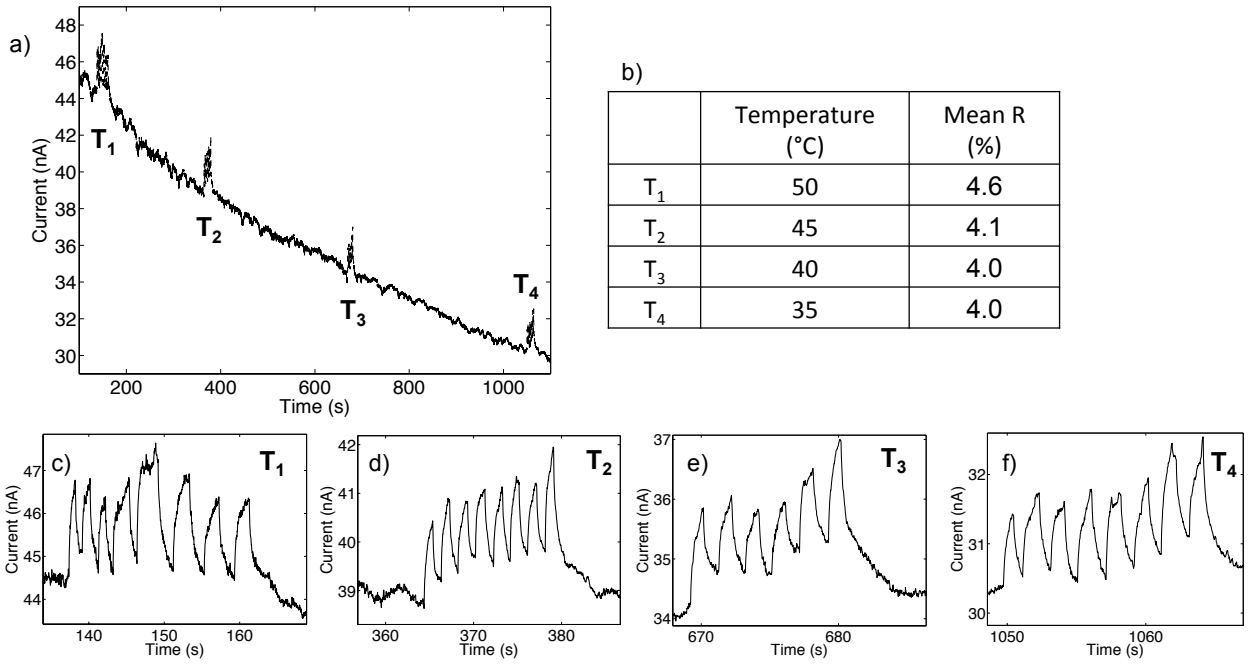

b)

	Temperature (°C)	Mean R (%)
T_1	50	4.6
T_2	45	4.1
T_3	40	4.0
T_4	35	4.0

Figure 4.7 a) Temperature-dependent current-time measurements under NIR chopped light (λ_{exc}=980 nm, power density $\approx$ 5 W/cm^2) for 8 mol % UCNP/WO_3. Thin films were deposited on patterned ITO with an interelectrode distance of 100 μm and thermally treated at 385°C. b) Table showing the evolution of the substrate temperature and the on/off ratio R. Temperature-dependent current-time measurements at c) T_1=50°C, d) T_2=45°C, e) T_3=40°C and f) T_4=35°C.

4.5 Results on $LiYF_4$: Tm^{3+}, Yb^{3+} UCNPs

In this section, results on the use of $LiYF_4$: Tm^{3+}, Yb^{3+} UCNPs with WO_3 are presented. The main motivation behind this set of experiments is to use UCNPs with emission properties that better match the absorption of the WO_3 (with respect to $NaGdF_4$: Er^{3+}, Yb^{3+} and WO_3). We expected a higher photocurrent in $LiYF_4$: Tm^{3+}, Yb^{3+}/WO_3 than in $NaGdF_4$: Er^{3+}, Yb^{3+}/WO_3 thin films.

The experimental details are the same than in chapter 2. WO_3 was prepared via a sol-gel process, and $LiYF_4$: Tm^{3+}, Yb^{3+} UCNPs by a thermal decomposition process, similarly to the preparation of $NaGdF_4$: Er^{3+}, Yb^{3+} UCNPs. A mixture made from these two solutions was used to produce thin films deposited on ITO-patterned electrodes (L = 100μm) and thermally treated at 385°C.

The morphology and size distribution of the $LiYF_4$: Tm^{3+}, Yb^{3+} UCNPs are shown on

figure 4.8. The shape of the UCNPs is rather elongated compared to $NaGdF_4$: Er^{3+}, Yb^{3+}. Their average length and width are 105 nm, and 60 nm.

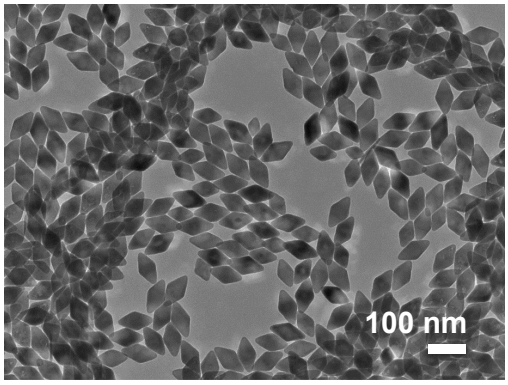

Figure 4.8 TEM image of $LiYF_4$: Tm^{3+}, Yb^{3+} UCNPs. This image was collected by Dr. Marta Quintanilla (INRS-EMT, Prof. F. Vetrone's research group).

The PL properties of pure $LiYF_4$: Tm^{3+}, Yb^{3+} UCNPs are shown on figure 4.9. Under 980 nm, UCNPs show four emission bands, centered at ca. 350, 490, 650, and 800 nm. The effect of the thermal treatment on the PL properties of $LiYF_4$: Yb^{3+}, Yb^{3+} is currently investigated.

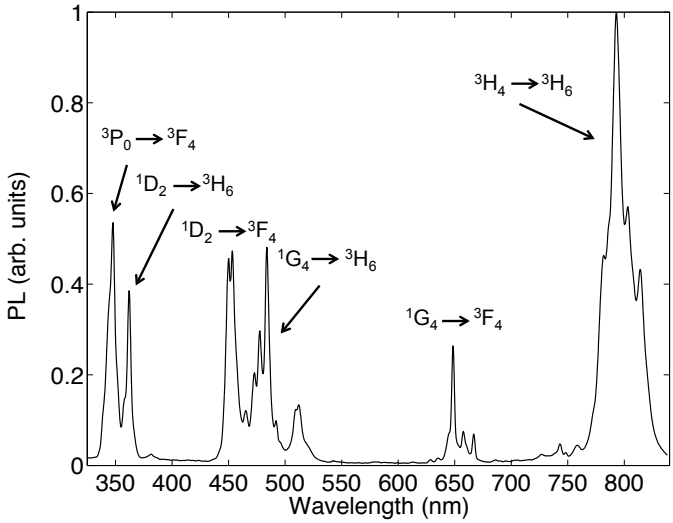

Figure 4.9 Photoluminescence properties of $LiYF_4$: Tm^{3+}, Yb^{3+} UCNPs, drop-cast on a glass substrate and dried at RT.

The structure of the UCNPs powder was investigated with XRD measurements, as shown on figure 4.10. The peaks are indexed to the hexagonal phase of the UCNPs [6]. We still have to determine what is the impact of a thermal treatment on the structure of the UCNPs.

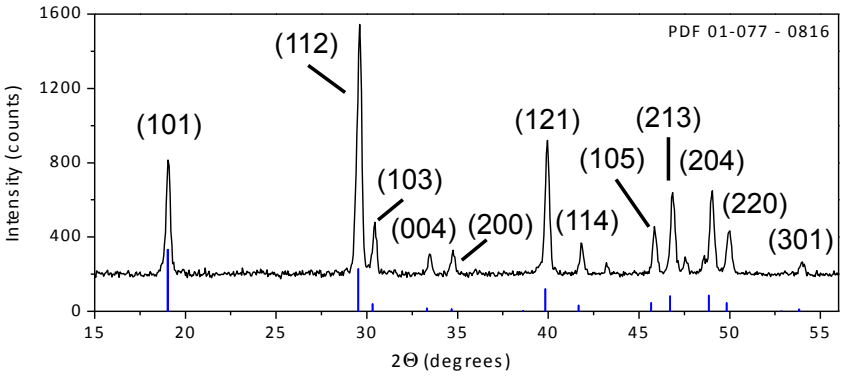

Figure 4.10 XRD pattern of the $LiYF_4$: Tm^{3+}, Yb^{3+} powder. The peaks are indexed to the hexagonal phase [6]. This measurement was performed by Dr. Marta Quintanilla (INRS-EMT, Prof. F. Vetrone's research group).

Finally, the electrical properties under λ_{exc}=980 nm irradiation of the thin films made of $LiYF_4$: Tm^{3+}, Yb^{3+} and WO_3 and thermally treated at 385°C are shown on figure 4.11. There is an increase in the current measured when a 980 nm laser irradiates the sample under constant electrical bias (0.5 V). The ratio R is about 4 %.

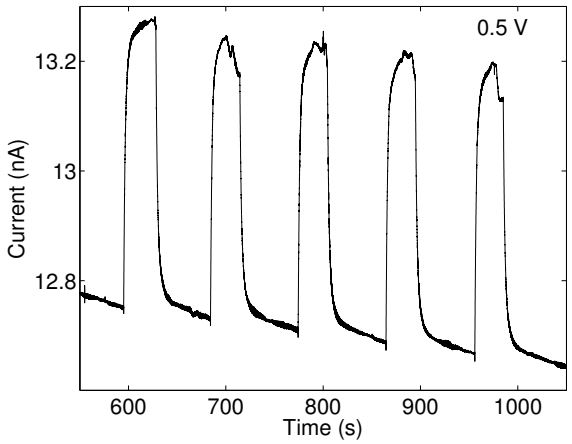

Figure 4.11 Current-time measurements under NIR chopped light (λ_{exc}=980 nm, power density ≈1 W/cm^2) of $LiYF_4$: Tm^{3+}, Yb^{3+}/WO_3 thin films deposited on patterned ITO electrodes ($L = 100\mu$m) and thermally treated at 385°C.

CHAPTER 5 GENERAL DISCUSSION

The work presented in this master's thesis was motivated by the three objectives stated in section 1.3. We were interested in producing thin films containing a known $NaGdF_4$: Er^{3+}, Yb^{3+} UCNPs/WO_3 mol% ratio. Several ratios have been investigated and we found that 8 mol% UCNP/WO_3 was the most interesting from the point of view of photocurrent generation. We characterized the morphology and structure of the thin films produced to assess their possible integration in solar energy conversion devices. We also shed light on the mechanism of generation of current under irradiation.

In this section, we discuss contributions that we consider of essential importance and that we could not easily control during the relatively short time a master's project usually takes. These contributions deserve attention for a better understanding of the photosensitization process and their study will be the object of further research in Pr. Santato group.

1. **AGING**: First, we would like to discuss the presence of an aging process in the precursor solutions used to fabricate the films. In the case of the WO_3 sol, aging results from the partial evaporation of the solvents and gelification. For example, films made from 'fresh' (ca. 6 hour old) WO_3 sol were normally thin (< 500 nm), while films made from a WO_3 sol aged for 48h were usually thick (800 nm to 1 μm). For the mixture made from UCNPs and WO_3, the aging time was usually 1 hour. When aged for more than 24 h, the UCNP/WO_3 precursors tend to precipitate and become unuseful for the production of the films.

   UCNPs are known to be chemically stable. Nevertheless, the possible evolution of the emission properties of the UCNPs evolve is largely undiscovered. For instance, we do not know if freshly prepared UCNPs ($<$ 1 week) have different PL properties than 6 month-old UCNPs. We do know after a number of discussion with our scientific collaborators at INRS-EMT that UCNPs tend to aggregate after some time. For this reason, UCNPs were always put in an ultrasonic bath for 15 minutes prior to the preparation of the UCNP/WO_3 precursor.

2. **THICKNESS OF THE NANOCOMPOSITE FILM**: We typically observed a better photosensitization in thick films (ca. 1 μm). An interesting experiment would be to conduct a systematic investigation to see to which extent the value of the ratio R (equation 3.1) depends on the thickness of the UCNP/WO_3 thin films.

3. **UCNPSs SIZE**: Most of the results were obtained with 45 nm sized $NaGdF_4$: Er^{3+}, Yb^{3+} UCNPs. For nanocomposite thin films made of 95 nm sized $NaGdF_4$: Er^{3+}, Yb^{3+} UCNPs, we did not observe an increase in current upon 980 nm irradiation. It is known that UCNPs size has an effect on the PL properties. For instance, very small (e.g. 15 nm) UCNPs are more sensitive to surface defects, which results in a weaker emission. Systematic comparison of the photosensitization of WO_3 and the size of the UCNPs could guide further work in order to find what is the optimal UCNPs size for WO_3 photosensitization.

4. **SPATIAL DISTRIBUTION OF UCNPs IN THE NANOCOMPOSITE FILMS**: From the AFM survey, we did not observe a segregation of UCNPs or WO_3. However, AFM is sensitive to the surface of the sample, so we do not know how UCNPs are distributed throughout the volume of the films.

5. **PHOTOSENSITIZATION MECHANISM**: Results seem to suggest that what we observed can be associated to an optical processes, rather than thermal processes. According to the work done during this master's project, results support a possible mechanism based on the absorption of NIR light by UCNPs that emit photons harvested by WO_3, to eventually generate a photocurrent. However, we cannot rule out other mechanisms. For instance, a non-radiative energy transfer between the UCNPs and WO_3 could take place. UCNPs, while in their excited state, could interact with WO_3 through non-radiative processes, such as in Förster resonance energy transfer. Experiments are ongoing in collaboration with our colleagues at INRS-EMT to shed light on this issue.

CHAPTER 6 CONCLUSIONS AND PERSPECTIVES

6.1 Conclusions

In this work, we tried to assess the possibility to produce two-component thin films made of $NaGdF_4$: Er^{3+}, Yb^{3+} and WO_3 in order to photosensitize the WO_3 to the NIR portion of the solar spectrum. We expected that under NIR irradiation, UCNPs absorb and upconvert NIR light that could be harvested by WO_3 to generate a photocurrent. As stated by the objectives presented in section 1.3, we were first interested in producing thin films containing a mixture of UCNPs and WO_3 in a given ratio.

We had to optimize the UCNPs/WO_3 mol/mol ratio and the temperature of the thermal treatment of the thin films. Films made of 8 mol/mol % UCNP/WO_3 thermally treated at 385°C were shown to be the most interesting from the point of view of the current generated under 980 nm irradiation. The temperature of the thermal treatment was selected to obtain crystalline WO_3 for good charge carrier transport and hexagonal $NaGdF_4$: Er^{3+}, Yb^{3+} for good photosensitization. XRD measurements confirmed that the UCNPs did not undergo a phase change after the thermal treatment at 385°C. 8 mol % UCNP/WO_3 thin films were smooth and continuous on the substrate surface. Values for the parameter R (defined in the equation 3.1) ranging from 3.4 to 3.9 % were obtained when 980 nm laser was shed on 8 mol% UCNP/WO_3 thin films under a constant bias (ranging between 0.5 and 1.0 V).

We also studied the possibility that thermal effects due to the laser exposure were responsible for the current increase observed, so pure WO_3 films were exposed to the NIR laser. We observed no noticeable current increase in this case. These results suggest that the increase in current reported in 8 mol% UCNP/WO_3 under NIR exposure is likely a real photocurrent. In this scenario, UCNPs would absorb the NIR light, WO_3 harvest the upconverted light, eventually generating a photocurrent.

6.2 Perspectives

The following experiments could be completed in a near future:

1. Complete the electrical characterization of $NaGdF_4$: Er^{3+}, Yb^{3+} UCNP/WO_3 thin films using a planar configuration under simulated solar light;

2. Determine if the temperature of the thermal treatment affects the PL properties and the structure of blue-emitting $LiYF_4$: Tm^{3+}, Yb^{3+} UCNPs. PL properties and crystalline structure should be carefully characterized;

3. Find the optimal mol/mol ratio between the $LiYF_4$: Tm^{3+}, Yb^{3+} UCNPs and the WO_3, in such a way that the photosensitization and charge carrier transport properties of the thin films are optimized;

4. Perform the electrical characterization of nanocomposite thin films (containing $NaGdF_4$: Er^{3+}, Yb^{3+}or $LiYF_4$: Tm^{3+}, Yb^{3+} UCNPs) using a vertical ("sandwiched") configuration under NIR monochromatic laser and simulated solar light.

5. Develop a better understanding of the interaction between the UCNPs and WO_3 by elucidating the mechanisms involved in the generation of the photocurrent. A possible mechanism is the absorption of NIR light by UCNPs, that emit photons to be absorbed by WO_3, thus generating a photocurrent. Another mechanism could be based on energy transfer between the UCNPs and WO_3, as in Förster resonance energy transfer. In this scenario, the UCNPs, while in their excited state, could interact with WO_3 through non-radiative processes.

BIBLIOGRAPHY

[1] H. Zhou, Y. Qu, T. Zeid, and X. Duan, "Towards highly efficient photocatalysts using semiconductor nanoarchitectures," *Energy & Environmental Science*, vol. 5, no. 5, pp. 6732–6743, 2012.

[2] P. Ramasamy, P. Manivasakan, and J. Kim, "Upconversion nanophosphors for solar cell applications," *RSC Advances*, vol. 4, no. 66, pp. 34873–34895, 2014.

[3] W. Shockley and H. J. Queisser, "Detailed balance limit of efficiency of p-n junction solar cells," *Journal of Applied Physics*, vol. 32, no. 3, pp. 510–519, 1961.

[4] J.-C. Boyer and F. C. J. M. van Veggel, "Absolute quantum yield measurements of colloidal $NaYF_4$: Er^{3+}, Yb^{3+} upconverting nanoparticles.," *Nanoscale*, vol. 2, pp. 1417–1419, 2010.

[5] R.-g. Yang, N. Xi, K. W.-c. Lai, B.-h. Zhong, C. K.-m. Fung, C.-g. Qu, and D. H. Wang, "Nanomechanical analysis of insulinoma cells after glucose and capsaicin stimulation using atomic force microscopy.," *Acta pharmacologica Sinica*, vol. 32, no. 6, pp. 853–860, 2011.

[6] G. Brunton, H. Insley, T. McVay, and R. Thoma tech. rep., ORNL-3761; United States Atomic Energy Commission: 1965.

[7] M. Green, "Photovoltaics: coming of age," in *Photovoltaic Specialists Conference, 1990., Conference Record of the Twenty First IEEE*, (Kissimmee, Florida), 1990.

[8] T. F. Schulze and T. W. Schmidt, "Photochemical upconversion : Present status and prospects for its application to solar energy conversion," *Energy & Environmental Science*, vol. 8, pp. 103–125, 2014.

[9] K. Kalyanasundaram and M. Grätzel, "Themed issue: nanomaterials for energy conversion and storage," *Journal of Materials Chemistry*, vol. 22, no. 46, pp. 24190–24194, 2012.

[10] H. Águas, S. K. Ram, A. Araújo, D. Gaspar, A. Vicente, S. a. Filonovich, E. Fortunato, R. Martins, and I. Ferreira, "Silicon thin film solar cells on commercial tiles," *Energy & Environmental Science*, vol. 4, no. 11, pp. 4620–4632, 2011.

[11] A. Hagfeldt, G. Boschloo, L. Sun, L. Kloo, and H. Pettersson, "Dye-sensitized solar cells.," *Chem. Rev.*, vol. 110, no. 11, pp. 6595–6663, 2010.

[12] N. Ashcroft and N. Mermin, *Solid State Physics*. Philadelphia: Saunders College, 1976.

[13] Z. I. Alferov, V. Andreev, M. Kagan, I. Protasov, and V. Trofim, "Solar-energy converters based on p-n $Al_xGa_{1-x}As$-GaAs heterojunctions," *Soviet Physics Semiconductor - USSR*, vol. 4, no. 12, pp. 2047–2048, 1971.

[14] D. A. Cusano, "CdTe solar cells and photovoltaic heterojunctions in II VI compounds," *Solid State Electronics*, vol. 6, no. 3, pp. 217–218, 1963.

[15] M. A. Green, "Third generation photovoltaics: solar cells for 2020 and beyond," *Physica E: Low-dimensional Systems and Nanostructures*, vol. 14, no. 1, pp. 65–70, 2002.

[16] E. D. Jackson, "Areas for improvement of the semiconductor solar energy converter," in *Proc. Conf. on the Use of Solar Energy*, (Tucson, Arizona), pp. 122–126, 1955.

[17] G. Conibeer, "Third-generation photovoltaics," *Materials Today*, vol. 10, no. 11, pp. 42–50, 2007.

[18] B. Richards, X. H. Geng, Y. H. Mai, G. F. Hou, Y. Zhao, J. M. Xue, X. D. Zhang, H. Z. Ren, J. Sun, and D. K. Zhang, "3C-SiC as a future photovoltaic material," in *Proceedings of 3rd World Conference on Photovoltaic Energy Conversion*, vol. A-C, (Osaka), pp. 1722–1724, 2003.

[19] M. J. Keevers and M. a. Green, "Extended infrared response of silicon solar cells and the impurity photovoltaic effect," *Solar Energy Materials and Solar Cells*, vol. 41-42, pp. 195–204, 1996.

[20] R. T. Ross and A. J. Nozik, "Efficiency of hot-carrier solar energy converters," *Journal of Applied Physics*, vol. 53, no. 5, pp. 3813–3818, 1982.

[21] P. Würfel, "Solar energy conversion with hot electrons from impact ionisation," *Solar Energy Materials and Solar Cells*, vol. 46, no. 1, pp. 43–52, 1997.

[22] M. Hanna and A. Nozik, "Solar conversion efficiency of photovoltaic and photoelectrolysis cells with carrier multiplication absorbers," *Journal of Applied Physics*, vol. 100, no. 7, pp. 074510–1–074510–8, 2006.

[23] R. D. Schaller and V. I. Klimov, "High efficiency carrier multiplication in pbse nanocrystals: implications for solar energy conversion," *Physical Review Letters*, vol. 92, no. 18, pp. 186601–1–186601–4, 2004.

[24] H.-Q. Wang, M. Batentschuk, A. Osvet, L. Pinna, and C. J. Brabec, "Rare-Earth Ion Doped Up-Conversion Materials for Photovoltaic Applications," *Advanced Materials*, vol. 23, no. 23, pp. 2675–2680, 2011.

[25] T. Trupke, A. Shalav, B. Richards, P. Würfel, and M. Green, "Efficiency enhancement of solar cells by luminescent up-conversion of sunlight," *Solar Energy Materials and Solar Cells*, vol. 90, no. 18-19, pp. 3327–3338, 2006.

[26] P. V. Kamat, "Quantum Dot Solar Cells. Semiconductor Nanocrystals as Light Harvesters," *Journal of Physical Chemistry C*, vol. 112, no. 48, pp. 18737–18753, 2008.

[27] A. J. Nozik, M. C. Beard, J. M. Luther, M. Law, R. J. Ellingson, and J. C. Johnson, "Semiconductor quantum dots and quantum dot arrays and applications of multiple exciton generation to third-generation photovoltaic solar cells," *Chemical Reviews*, vol. 110, no. 11, pp. 6873–6890, 2010.

[28] B. Kippelen and J.-L. Brédas, "Organic photovoltaics," *Energy & Environmental Science*, vol. 2, no. 3, pp. 251–261, 2009.

[29] B. O'Regan and M. Grätzel, "A low-cost, high-efficiency solar cell based on dye-sensitized colloidal TiO_2 films," *Nature*, vol. 353, no. 6346, pp. 737–740, 1991.

[30] M. Matsumura, Y. Nomura, and H. Tsubomura, "Dye-sensitization on the photocurrent at zinc oxide electrode in aqueous electrolyte solution," *Bulletin of the Chemical Society of Japan*, vol. 50, no. 10, pp. 2533–2537, 1977.

[31] H. Witzke, S. Chen, S. Deb, and M. Russak, "Triple electrode photogalvanic cell with energy storage capability," Oct. 3 1978. US Patent 4,118,546.

[32] N. Alonso V., M. Beley, P. Chartier, and V. Ern, "Dye sensitization of ceramic semiconducting electrodes for photoelectrochemical conversion," *Revue de Physique Appliquée*, vol. 16, no. 1, pp. 5–10, 1981.

[33] X. Chen and S. S. Mao, "Titanium dioxide nanomaterials: Synthesis, properties, modifications and applications," *Chemical Reviews*, vol. 107, no. 7, pp. 2891–2959, 2007.

[34] H. Ishihara, G. K. Kannarpady, K. R. Khedir, J. Woo, S. Trigwell, and A. S. Biris, "A novel tungsten trioxide (WO_3)/ITO porous nanocomposite for enhanced photo-catalytic water splitting," *Physical Chemistry Chemical Physics*, vol. 13, no. 43, pp. 19553–19560, 2011.

[35] H. Zheng, J. Z. Ou, M. S. Strano, R. B. Kaner, A. Mitchell, and K. Kalantar-zadeh, "Nanostructured Tungsten Oxide - Properties, Synthesis, and Applications," *Advanced Functional Materials*, vol. 21, no. 12, pp. 2175–2196, 2011.

[36] D. Koziej, A. Lauria, and M. Niederberger, "25$^{\text{th}}$ Anniversary Article: Metal Oxide Particles in Materials Science: Addressing All Length Scales.," *Advanced materials*, vol. 26, no. 2, pp. 235–257, 2014.

[37] C. G. Granqvist, *Handbook of Inorganic Electrochromic Materials*. Elsevier, 1995.

[38] S. H. Baeck, K. S. Choi, T. F. Jaramillo, G. D. Stucky, and E. W. McFarland, "Enhancement of photocatalytic and electrochromic properties of electrochemically fabricated mesoporous WO_3 thin films," *Advanced Materials*, vol. 15, no. 15, pp. 1269–1273, 2003.

[39] S. Cong, Y. Tian, Q. Li, Z. Zhao, and F. Geng, "Single-Crystalline Tungsten Oxide Quantum Dots for Fast Pseudocapacitor and Electrochromic Applications.," *Advanced Materials*, vol. 26, no. 25, pp. 4260–4267, 2014.

[40] N. Bloembergen, "Solid state infrared quantum counters," *Phys. Rev. Lett.*, vol. 2, no. 3, pp. 84–85, 1959.

[41] F. Auzel, "Upconversion and anti-Stokes processes with f and d ions in solids.," *Chemical Reviews*, vol. 104, no. 1, pp. 139–173, 2004.

[42] W. G. van Sark, J. de Wild, J. K. Rath, A. Meijerink, and R. E. Schropp, "Upconversion in solar cells.," *Nanoscale Research Letters*, vol. 8, no. 1, pp. 81–90, 2013.

[43] J. de Wild, A. Meijerink, J. K. Rath, W. G. J. H. M. van Sark, and R. E. I. Schropp, "Upconverter solar cells: materials and applications," *Energy & Environmental Science*, vol. 4, no. 12, pp. 4835–4848, 2011.

[44] R. Naccache, Q. Yu, and J. a. Capobianco, "The Fluoride Host: Nucleation, Growth, and Upconversion of Lanthanide-Doped Nanoparticles," *Advanced Optical Materials*, vol. 3, no. 4, pp. 1–28, 2015.

[45] M. Haase and H. Schäfer, "Upconverting nanoparticles," *Angewandte Chemie - International Edition*, vol. 50, no. 26, pp. 5808–5829, 2011.

[46] A. Aebischer, S. Heer, D. Biner, K. Krämer, M. Haase, and H. U. Güdel, "Visible light emission upon near-infrared excitation in a transparent solution of nanocrystalline β-$NaGdF_4$: Yb^{3+}, Er $^{3+}$," *Chemical Physics Letters*, vol. 407, no. 1-3, pp. 124–128, 2005.

[47] B. M. van der Ende, L. Aarts, and A. Meijerink, "Lanthanide ions as spectral converters for solar cells.," *Physical Chemistry Chemical Physics : PCCP*, vol. 11, no. 47, pp. 11081–11095, 2009.

[48] J. C. Goldschmidt and S. Fischer, "Upconversion for Photovoltaics - a Review of Materials, Devices and Concepts for Performance Enhancement," *Advanced Optical Materials*, vol. 3, no. 4, pp. 510–535, 2015.

[49] T. Fix, G. Ferblantier, H. Rinnert, and a. Slaoui, "Evaluation of the effective quantum efficiency of photon conversion layers placed on solar cells," *Solar Energy Materials and Solar Cells*, vol. 132, pp. 191–195, 2015.

[50] F. Gibart, F. Auzel, J. Guillaume, and K. Zahraman, "Below band-gap IR response of substrate-free GaAs solar cells using two-photon up-conversion," *Japanese Journal of Applied Physics*, vol. 35, no. 8R, pp. 4401–4402, 1996.

[51] T. Trupke, M. A. Green, and P. Würfel, "Improving solar cell efficiencies by up-conversion of sub-band-gap light," *Journal of Applied Physics*, vol. 92, no. 7, pp. 4117–4122, 2002.

[52] A. Shalav, B. S. Richards, T. Trupke, K. W. Krämer, and H. U. Güdel, "Application of $NaYF_4$: Er^{3+} up-converting phosphors for enhanced near-infrared silicon solar cell response," *Applied Physics Letters*, vol. 86, no. 1, pp. 4–7, 2005.

[53] X. F. Liang, X. Y. Huang, and Q. Y. Zhang, "$Gd_2(MoO_4)_3$:Er^{3+} nanophosphors for an enhancement of silicon solar-cell near-infrared response," *Journal of Fluorescence*, vol. 19, no. 2, pp. 285–289, 2009.

[54] J. De Wild, J. K. Rath, a. Meijerink, W. G. J. H. M. Van Sark, and R. E. I. Schropp, "Enhanced near-infrared response of a-Si:H solar cells with β-$NaYF_4$:Yb^{3+} (18%), Er^{3+} (2%) upconversion phosphors," *Solar Energy Materials and Solar Cells*, vol. 94, no. 12, pp. 2395–2398, 2010.

[55] J. De Wild, A. Meijerink, J. K. Rath, W. G. J. H. M. Van Sark, and R. E. I. Schropp, "Towards upconversion for amorphous silicon solar cells," *Solar Energy Materials and Solar Cells*, vol. 94, no. 11, pp. 1919–1922, 2010.

[56] G.-B. Shan and G. P. Demopoulos, "Near-infrared sunlight harvesting in dye-sensitized solar cells via the insertion of an upconverter-TiO_2 nanocomposite layer.," *Advanced Materials*, vol. 22, no. 39, pp. 4373–4377, 2010.

[57] J. Wu, J. Wang, J. Lin, Z. Lan, Q. Tang, M. Huang, Y. Huang, L. Fan, Q. Li, and Z. Tang, "Enhancement of the Photovoltaic Performance of Dye-Sensitized Solar Cells by Doping $Y_{0.78}Yb_{0.20}Er_{0.02}F_3$ in the Photoanode," *Advanced Energy Materials*, vol. 2, no. 1, pp. 78–81, 2012.

[58] L. Liang, Y. Liu, and X.-Z. Zhao, "Double-shell β-$NaYF_4$:Yb^{3+}, Er^{3+}/SiO_2/TiO_2 submicroplates as a scattering and upconverting layer for efficient dye-sensitized solar cells.," *Chemical Communications*, vol. 49, no. 38, pp. 3958–3960, 2013.

[59] L. Liang, Y. Liu, C. Bu, K. Guo, W. Sun, N. Huang, T. Peng, B. Sebo, M. Pan, W. Liu, S. Guo, and X.-Z. Zhao, "Highly uniform, bifunctional core/double-shell-structured β-$NaYF_4$:Er^{3+}, Yb^{3+} @ SiO_2@TiO_2 hexagonal sub-microprisms for high-performance dye sensitized solar cells.," *Advanced Materials*, vol. 25, no. 15, pp. 2174–2180, 2013.

[60] Z. Zhou, J. Wang, F. Nan, C. Bu, Z. Yu, W. Liu, S. Guo, H. Hu, and X.-Z. Zhao, "Upconversion induced enhancement of dye sensitized solar cells based on core-shell structured β-$NaYF_4$:Er^{3+}, Yb^l3+@SiO_2 nanoparticles.," *Nanoscale*, vol. 6, no. 4, pp. 2052–2055, 2014.

[61] N. C. Dyck and G. P. Demopoulos, "Integration of upconverting β-$NaYF_4$:Yb^{3+}, Er^{3+} @TiO_2 composites as light harvesting layers in dye-sensitized solar cells," *RSC Adv.*, vol. 4, no. 95, pp. 52694–52701, 2014.

[62] A. Shalav, B. Richards, and M. Green, "Luminescent layers for enhanced silicon solar cell performance: Up-conversion," *Solar Energy Materials and Solar Cells*, vol. 91, no. 9, pp. 829–842, 2007.

[63] N. M. Idris, M. K. G. Jayakumar, A. Bansal, and Y. Zhang, "Upconversion nanoparticles as versatile light nanotransducers for photoactivation applications," *Chemical Society Reviews*, vol. 44, no. 6, pp. 1449–1478, 2014.

[64] T. F. Schulze and T. W. Schmidt, "Photochemical upconversion : Present status and prospects for its application to solar energy conversion," *Energy & Environmental Science*, vol. 8, no. 1, pp. 103–125, 2014.

[65] C. Santato, M. Odziemkowski, M. Ulmann, and J. Augustynski, "Crystallographically oriented mesoporous WO_3 films: synthesis, characterization, and applications.," *Journal of the American Chemical Society*, vol. 123, no. 43, pp. 10639–10649, 2001.

[66] J. Lemerle and J. Lefebvre, "Mise en évidence d'un nouvel acide tungstique en solution. Filiations avec d'autres polytungstates," *Canadian Journal of Chemistry*, vol. 55, no. 21, pp. 3758–3762, 1977.

[67] F. Vetrone, R. Naccache, V. Mahalingam, C. G. Morgan, and J. A. Capobianco, "The Active-Core/Active-Shell Approach: A Strategy to Enhance the Upconversion Luminescence in Lanthanide-Doped Nanoparticles," *Advanced Functional Materials*, vol. 19, no. 18, pp. 2924–2929, 2009.

[68] N. Bogdan, F. Vetrone, G. A. Ozin, and J. A. Capobianco, "Synthesis of ligand-free colloidally stable water dispersible brightly luminescent lanthanide-doped upconverting nanoparticles," *Nano Letters*, vol. 11, no. 2, pp. 835–840, 2011.

[69] T. M. Razykov, C. S. Ferekides, D. Morel, E. Stefanakos, and H. S. Ullal, "Solar photovoltaic electricity : Current status and future prospects," *Solar Energy*, vol. 85, no. 8, pp. 1580–1608, 2011.

[70] D. J. Friedman, "Progress and challenges for next-generation high-efficiency multijunction solar cells," *Current Opinion in Solid State and Materials Science*, vol. 14, no. 6, pp. 131–138, 2010.

[71] X. Huang, S. Han, W. Huang, and X. Liu, "Enhancing solar cell efficiency: the search for luminescent materials as spectral converters.," *Chemical Society Reviews*, vol. 42, no. 1, pp. 173–201, 2013.

[72] R. Naccache, F. Vetrone, and J. A. Capobianco, "Lanthanide-doped upconverting nanoparticles: Harvesting light for solar cells," *ChemSusChem*, vol. 6, no. 8, pp. 1308–1311, 2013.

[73] S. K. Deb, "Opportunities and challenges in science and technology of WO_3 for electrochromic and related applications," *Solar Energy Materials and Solar Cells*, vol. 92, no. 2, pp. 245–258, 2008.

[74] H. Zheng, Y. Tachibana, and K. Kalantar-Zadeh, "Dye-sensitized solar cells based on WO_3," *Langmuir*, vol. 26, no. 24, pp. 19148–19152, 2010.

[75] I. Concina and A. Vomiero, "Metal Oxide Semiconductors for Dye- and Quantum-Dot-Sensitized Solar Cells," *Small*, vol. 11, no. 15, pp. 1744–1774, 2015.

[76] L. Wang, R. Yan, Z. Huo, L. Wang, J. Zeng, J. Bao, X. Wang, Q. Peng, and Y. Li, "Fluorescence resonant energy transfer biosensor based on upconversion-luminescent nanoparticles," *Angewandte Chemie - International Edition*, vol. 44, no. 37, pp. 6054–6057, 2005.

[77] D. K. Chatterjee, A. J. Rufaihah, and Y. Zhang, "Upconversion fluorescence imaging of cells and small animals using lanthanide doped nanocrystals," *Biomaterials*, vol. 29, no. 7, pp. 937–943, 2008.

[78] R. Naccache, E. M. Rodríguez, N. Bogdan, F. Sanz-Rodríguez, M. del Carmen Iglesias de la Cruz, A. J. de la Fuente, F. Vetrone, D. Jaque, J. G. Solé, and J. A. Capobianco, "High resolution fluorescence imaging of cancers using lanthanide ion-doped upconverting nanocrystals," *Cancers*, vol. 4, no. 4, pp. 1067–1105, 2012.

[79] G. Feng, S. Liu, Z. Xiu, Y. Zhang, J. Yu, Y. Chen, P. Wang, and X. Yu, "Visible light photocatalytic activities of TiO_2 nanocrystals doped with upconversion luminescence agent," *Journal of Physical Chemistry C*, vol. 112, no. 35, pp. 13692–13699, 2008.

[80] S. Obregón and G. Colón, "Evidence of upconversion luminescence contribution to the improved photoactivity of erbium doped TiO_2 systems.," *Chemical Communications*, vol. 48, no. 63, pp. 7865–7867, 2012.

[81] M. Zhang, Y. Lin, T. J. Mullen, W.-f. Lin, L.-D. Sun, C.-H. Yan, T. E. Patten, D. Wang, and G.-Y. Liu, "Improving Hematite's Solar Water Splitting Efficiency by Incorporating Rare-Earth Upconversion Nanomaterials," *The Journal of Physical Chemistry C*, vol. 3, no. 21, pp. 3188–3192, 2012.

[82] Z. Xu, M. Quintanilla, F. Vetrone, A. O. Govorov, M. Chaker, and D. Ma, "Harvesting Lost Photons: Plasmon and Upconversion Enhanced Broadband Photocatalytic Activity in Core@Shell Microspheres Based on Lanthanide-Doped $NaYF_4$, TiO_2, and Au," *Advanced Functional Materials*, vol. 25, no. 20, pp. 2950–2960, 2015.

[83] S. Fischer, J. C. Goldschmidt, P. Löper, G. H. Bauer, R. Brüggemann, K. Krämer, D. Biner, M. Hermle, and S. W. Glunz, "Enhancement of silicon solar cell efficiency by upconversion: Optical and electrical characterization," *Journal of Applied Physics*, vol. 108, no. 4, pp. 1–11, 2010.

[84] R. Martín-Rodríguez, S. Fischer, A. Ivaturi, B. Froehlich, K. W. Krämer, J. C. Goldschmidt, B. S. Richards, and A. Meijerink, "Highly Efficient IR to NIR Upconversion in $Gd_2O_2S:Er^{3+}$ for Photovoltaic Applications," *Chemistry of Materials*, vol. 25, no. 9, pp. 1912–1921, 2013.

[85] J. F. Suyver, J. Grimm, M. K. van Veen, D. Biner, K. W. Krämer, and H. U. Güdel, "Upconversion spectroscopy and properties of $NaYF_4$ doped with Er^{3+}, Tm^{3+} and/or Yb^{3+}," *Journal of Luminescence*, vol. 117, no. 1, pp. 1–12, 2006.

[86] C. Yuan, G. Chen, P. N. Prasad, T. Y. Ohulchanskyy, Z. Ning, H. Tian, L. Sun, and H. Å gren, "Use of colloidal upconversion nanocrystals for energy relay solar cell light harvesting in the near-infrared region," *Journal of Materials Chemistry*, vol. 22, no. 33, pp. 16709–16713, 2012.

[87] A. F. Khan, R. Yadav, P. K. Mukhopadhya, S. Singh, C. Dwivedi, V. Dutta, and S. Chawla, "Core-shell nanophosphor with enhanced NIR-visible upconversion as spectrum modifier for enhancement of solar cell efficiency," *Journal of Nanoparticle Research*, vol. 13, no. 12, pp. 6837–6846, 2011.

[88] A. Moadhen, C. Bouzidi, H. Elhouichet, R. Chtourou, and M. Oueslati, "Concentration and temperature dependence of visible up-conversion luminescence in sol-gel SnO_2 doped with erbium," *Optical Materials*, vol. 31, no. 8, pp. 1224–1227, 2009.

[89] J. Zhang, H. Shen, W. Guo, S. Wang, C. Zhu, F. Xue, J. Hou, H. Su, and Z. Yuan, "An upconversion $NaYF_4$:Yb^{3+},Er $^{3+}$/TiO_2 core-shell nanoparticle photoelectrode for improved efficiencies of dye-sensitized solar cells," *Journal of Power Sources*, vol. 226, pp. 47–53, 2013.

[90] J. Wang, J. Lin, J. Wu, M. Huang, Z. Lan, Y. Chen, S. Tang, L. Fan, and Y. Huang, "Application of Yb3+, Er3+-doped yttrium oxyfluoride nanocrystals in dye-sensitized solar cells," *Electrochimica Acta*, vol. 70, pp. 131–135, 2012.

[91] L. Li, Y. Yang, R. Fan, Y. Jiang, L. Wei, Y. Shi, J. Yu, S. Chen, P. Wang, B. Yang, and W. Cao, "A simple modification of near-infrared photon-to-electron response with fluorescence resonance energy transfer for dye-sensitized solar cells," *Journal of Power Sources*, vol. 264, pp. 254–261, Oct. 2014.

[92] C. Rüssel, "A pyrolytic route to fluoride glasses. I. Preparation and thermal decomposition of metal trifluoroacetates," *Journal of Non-Crystalline Solids*, vol. 152, no. 2-3, pp. 161–166, 1993.

[93] B. Yang, Y. Zhang, E. Drabarek, P. R. F. Barnes, and V. Luca, "Enhanced Photoelectrochemical Activity of Sol - Gel Tungsten Trioxide Films through Textural Control," *Chem. Mater.*, vol. 19, no. 23, pp. 5664–5672, 2007.

[94] P. Chen, M. Song, E. Wu, B. Wu, J. Zhou, H. Zeng, X. Liu, and J. Qiu, "Polarization modulated upconversion luminescence: single particle vs. few-particle aggregates," *Nanoscale*, vol. 7, no. 15, pp. 6462–6466, 2015.

[95] L. H. Fischer, G. S. Harms, and O. S. Wolfbeis, "Upconverting nanoparticles for nanoscale thermometry.," *Angewandte Chemie (International ed.)*, vol. 50, no. 20, pp. 4546–4551, 2011.

APPENDIX A Theoretical estimation of the photocurrent generated in 8 mol % $NaGdF_4$: Er^{3+}, Yb^{3+} UCNP/WO_3 thin films

Let us define α as the absorption coefficient of $NaGdF_4$: Er^{3+}, Yb^{3+} UCNP, UCQY as upconversion quantum yield, and η_{WO_3} as the absorption of WO_3 at 550 nm (which corresponds to one emission band of UCNPs). Assuming the following values:

$$\alpha \approx 0.02 \text{ cm}^{-1}$$

$$\text{UCQY} \approx 0.001$$

$$\eta_{WO_3} \approx 0.15$$

We can define X by:

$$X = \frac{\#\text{UCNPs in the film}}{\text{cm}^3} \times \text{laser spot area} \times \text{thickness (of the film)}$$

We can also define Y:

$$Y = \alpha \times X \times \text{thickness of the UCNPs}$$

Let us assume that the thickness of the UCNPs $\approx$ 50 nm and that they are all in the same direction (perpendicular to the surface).

Now, let us define $P_{\text{photocurrent}}$, the increase in current when the sample is placed under 980 nm irradiation:

$$P_{\text{photocurrent}} = \eta_{WO_3} \times Y \times \text{UCQY}$$

Let us find $\frac{\#\text{UCNPs in the film}}{\text{cm}^3}$:

We know that 8 mol/mol % ratio refers to Gd/WO_3 mol/mol ratio. In this scenario, there is $\approx$ 2 % of Yb^{3+} ions in the hybrid thin film. If we assume that the size of WO_3 particles is the same as the UCNPs ($\approx$ 50 nm), then:

The volume of 1 particle (assuming a cube for simplicity) is 1.25×10^{-22} m^3. It means that there are 8×10^{21} particles/ m^3, i.e. 8×10^{15} particles/ cm^3.

In this scenario, there are 1.74×10^{14} UCNPs/cm^3 and 7.82×10^{15} WO_3 particles/cm^3.

Let us assume that the laser spot area is 0.5 cm^2 and the thickness of the film $\approx$ 1000 nm (or 10^{-4} cm).

Then,

$$\begin{aligned} Y &= \alpha \times X \times \text{thickness of the UCNPs} \\ &= 0.02 \text{ cm}^{-1} \times \frac{1.74 \times 10^{14}}{\text{cm}^3} \times 0.5 \text{ cm}^2 \times 10^{-4} \text{ cm} \times 5 \times 10^{-6} \text{ cm} \\ &= 870 \end{aligned}$$

The increase in photocurrent $P_{\text{photocurrent}}$ is thus defined by:

$$\begin{aligned} P_{\text{photocurrent}} &= \eta_{WO_3} \times Y \times \text{UCQY} \\ &= 0.15 \times 870 \times 0.001 \\ &= 0.1305... \approx 13\% \end{aligned}$$

Under the assumptions that were made, the maximal photocurrent generated in 8 mol/mol % UCNP/WO_3 thin films should theoretically be around 13 %.